Laser-induced phase-structure changes (PSC) in glass-like materials

V. VEIKO[a], E. AGEEV[a], A.V. KOLOBOV[b*], J. TOMINAGA[b]

[a]National Research University of Information Technologies, Mechanics and Optics, Kronverkskiy pr., 49, 197101, Saint Petersburg, Russia
[b]Nanoelectronics Research Institute, National Institute of Advanced Industrial Science and Technology, Tsukuba Central 4, 1-1-1 Higashi, Tsukuba, Ibaraki 305-8562, Japan

This review makes an attempt to analyze the experiment and qualitative theoretical results related to fundamental photochemical and photophysical processes in laser machining of glasses and glass-ceramics, on the one hand, and phase-change memory alloys on the other hand, where a controllable laser exposure can locally change the properties of a material, e.g., its chemical solubility and transmittance in the visible and IR spectral ranges. In some cases, the process may be reversed, either thermally or by appropriately choosing the parameters of the laser exposure.

1. Introduction

Nowadays, phase-changing materials seem to be very promising and interesting, which has been evidenced by A. Kolobov [1], K. Sugioka et al. [2-7], H. Helvajian et al. [7-8], and V. Veiko et al. [9-11]. Even the results obtained in these studies demonstrate that materials of this kind can be applied in optical memory development, construction of nanosatellites, microfluidic, and photonic devices and, therefore have a great future. The physical principles of PSC, revealed in the studies mentioned above, make it basically possible to produce locally modified areas in most part of the known glasses in the present situation in this field of knowledge. Just this fact generates a frontier of "laser-based" materials sciences. One can speak about a stage, primarily for the photonics, passed at its time (in the 1950s) by the electronic engineering. Specifically, this is a transition to simultaneous generation of advanced materials and elements on a single substrate (microelectronics) instead of development of individual elements and their combination into assemblies (microassemblies). A phase transition from the amorphous state to a crystal and/or back (A-C, or C-A, or A-C-A, or C-A-C) could serve as a general-purpose element of this kind. It is possible to control the dimensions, depth of occurrence, switching time and other properties of this transition by light (laser beam). Equally revolutionary changes could be expected to occur on the basis of such advanced materials and approaches in microfluidics, microsystem devices (MEMS, MOEMS), and other up-to-date fields of instrument making. It is because of anticipating a new "wave" of knowledge and applications in this field that the authors decided that preparation and publication of this review is timely and it is reasonable to invite scientists' attention to the research in the aforementioned field.

Today, there are two large groups of materials of this kind. These are chalcogenide glasses (semiconductors) and silicate glasses or glass-ceramics (insulators). The type of the matrix of a material strongly affects properties of both groups, including their optical properties which are of prime importance for laser-induced-phase-change applications. As for the phase-changing materials reviewed in present the report, we identify such materials as materials in which laser-induced phase-structure changes take place.

Nematic liquid crystals constitute a familiar group of materials in which typical PSC occur under exposure to light, which results in that their structure and characteristics are changed. These materials are not considered in this review because of being extensively studied, with not only related articles but also monographs readily available [12-17]. In summary, this review deals with glass-like materials having two different states, amorphous and (poly)crystalline, which can be converted one into another (with a reversible transition, if possible), and thereby acquire new physicochemical properties, such as optical transparency, selective solubility, etc.

It is well known that lasers are a powerful tool for controlling surface characteristics of various materials. Some examples can be noted, such as the laser hardening of iron-carbon alloys (with the exception of laser pinning because of its being based on the quasi-volumetric action of penetrating shock waves) [18]; laser oxidation of thin chromium films to produce a selective solubility of irradiated and nonirradiated areas, which has been extensively used for fabrication of diffracting optical elements [19-21]; laser annealing of ion-implanted silicon

[22-24], etc. It should be mentioned that all of these operations are surface-modification processes.

It is apparent that involvement of the third dimension could impart novel capabilities to various applied technologies. The choice of a material suitable for this purpose seems to be clear. It should be optically transparent. And glasses can be used predominantly because of the well-developed physical and chemical aspects of their processing and the wide variety of their application. However, the good transparence of glasses is, at the same time, a restriction for their bulk (3D) modification (three-dimensional). It was necessary to develop ultrafast (picosecond and femtosecond) lasers, for which the linear absorption of radiation is still low, but there is a rapid rise in the photon density in proportion to the beam focusing. The increase in the photon density brings into existence high-order (higher than second and third) nonlinearities, which gives rise to new light absorption mechanisms (multiphoton absorption, avalanche ionization, etc.) and enables control over the glass properties. As a result, it becomes possible to pass from a 2D processing technology (formation of surface structures) to 3D structuring (development of structures in a bulk material). It is no coincidence that numerous studies on phenomena occurring within various glasses, photopolymers, and other unconventional materials have appeared at once.

Fabrication of 3D structures production necessitates that the material should be transparent for the operating wavelength and the interaction between the material and incident light occurs only in the focusing area. A significant advantage of this kind of processing is in its increased accuracy [26]. With femtosecond laser pulses (wavelength λ = 800 nm), various devices for biotechnology [27], micro-optics [28], and many other fields of technology can be fabricated from photosensitive glasses (PGs). Also, there have been reports about application of picosecond laser pulses [29, 30]. Earlier studies demonstrated that nanosecond UV lasers van be used for PG modification and development of various "microtools", such as gas electron multipliers [31], tips for atomic-force microscopy [32, 33], master stamps for polymer surfaces [34], capillary electrophoresis chips for separation of amino-acids [35], chemical microreactors [36, 37], etc.

In what follows we describe the physics and applications of photo-induced phenomena in two classes of materials, namely in photosensitive glasses and glass-ceramics and in so-called phase-change memory alloys.

2. Silicate phase –changing materials

2.1 Glass-ceramics and photosensitive glasses: different sides of the same coin

According to the general notion, the glass is a supercooled melt of an amorphous inorganic material, obtainable by melt-quenching of a glass-forming substance [38]. The glass-forming substances can be identified as inorganic substances which do not crystallize in melt-quenching and are solidified as an amorphous phase. Melts of glass-forming substances commonly have a higher viscosity in comparison with melts of non-glass-forming substances.

A solid glassy state is reached under constant-pressure cooling. The transition of a substance from the liquid state to a glass is reversible and occurs within a certain temperature range whose upper and lower limits correspond to viscosities of 10^{12} and 10^{8} Pa·s, respectively [38]. Also, the glassy state can be reached by condensation of a substance from a vapor stage (vacuum evaporation, plasma sputtering), hydrolysis of films, evaporation of liquids, and exposure of a crystalline material to high-velocity particles or to a shock wave. The industrial technique most frequently employed for commercial production of inorganic glasses is by melting of a mixture of starting materials and supercooling of the resulting melts.

Elements (S, Se, As, C, P), oxides (SiO_2, B_2O_3, P_2O_5, GeO_2, As_2O_3, etc.), and also binary, ternary, and multicomponent formulations based on glass-forming oxides, halides (BeF_2), chalcogenides (As_2S_3, Sb_2Se_3), sulfates, selenides, etc. can be obtained in the glassy state.

The glassy state of a substance is non-equilibrium and has larger values of entropy, enthalpy and, in general, specific volume than the crystalline state. The structure and properties of glasses depend on the chemical composition of the mixture of base substances, conditions of their synthesis, rate of supercooling within the glass-transition range, and additional thermal treatment processes.

The structural and phase modification of glassy materials by laser irradiation seems to be highly promising, because this technique can locally change characteristics of the initial environment and thereby can create its necessary functionality. A laser can provide a nonequilibrium non-stationary inhomogeneous exposure, which can potentially provide a local modification of an initially homogeneous material (formation of certain phases or altering of characteristics). The interested reader can find more details on use of laser-excitation to modify materials properties in the monograph appropriately titled "Materials Modification by Electronic Excitation [39].

In contrast to glasses, glass-ceramics are vitro-crystalline (micro- or nanocrystalline) materials produced by planar (catalyzed) crystallization of special-composition glasses. The glass-ceramics consist of one or several crystalline phases uniformly embedded in a glassy phase.

The main feature of the glass-ceramics is the fine-grained uniform vitro-crystalline structure that combines a high hardness and mechanical strength with excellent insulating properties, high softening temperature, and good thermal and chemical resistance. The thermal stability of some kinds of glass-ceramics is determined by the very small thermal-expansion coefficient [40], which may occasionally be even negative, (from $-7 \cdot 10^{-7}$ K^{-1} to $+3 \cdot 10^{-7}$ K^{-1}). The optical glass can be replaced with transparent glass-ceramics, which are advantageous in

that, having a small thermal-expansion coefficient, they are resistant to dramatic changes in temperature. The transparence of glass-ceramics to visible light is attributed to the size of crystals, which are smaller than half the wavelength of visible light (hundredths of a micrometer), and their refractive index is close to that of the glassy phase.

Such properties as the density, thermal-expansion coefficient, thermal conductivity, Young's modulus, and permittivity of glass-ceramics depend on the properties of the constituent phases and additively vary with the content of these phases (see, e.g., [40]). The substances serving as a catalyst and crystallization centers in glasses are necessary additives [40]. The role of such additives can be played by metals (Au, Ag, Cu, Pt, Pd in amounts of a hundredth to a tenth of a percent), oxides (TiO_2, P_2O_5, Cr_2O_3, ZrO_2, etc.), fluorides (Na_3AlF_6, Na_2SiF_6, CaF_2, etc.), sulfur or sulfates with addition of a carbonate, and sulfides.

The high-temperature resistance, electrical conductivity, and mechanical strength of glass-ceramics depend not only on properties of the constituent phases, but, even to a greater extent, on their structure and, consequently, they are not additive. The compact microstructure provides a high hardness and abrasion resistance. The increase in the degree of crystallinity makes larger the Young's modulus. The low content of the glassy phase improves the mechanical, thermal, and dielectric properties of the material and improves its chemical resistance.

There is another group of advanced materials, named photostructurable or photosensitive glasses (PG). The first PG material appeared in the late 1940s [42]. Since that time these materials have been attracting significant attention due to the unique opportunity to control structural phase transitions in these materials by photoactivation. Also important are such properties of these materials as the large Young's modulus, good chemical stability, high transmittance in the visible spectral range, etc. The PG composition includes a photosensitizer, which is the substance that promotes a fuller extent of photochemical processes and improves the photosensitivity, with a latent surface image formed. The role of photosensitizers can be played by CeO_2, monovalent gold, sulfides of alkali metals, etc., in which photoelectrons are generated by the absorbed UV light. During the thermal processing, these photoelectrons reduce metal ions to atoms. The diffusion coefficient of atoms in the lattice substantially exceeds that of ions, and this leads to fast formation of clusters of metal nanoparticles on which the crystalline phase grows. This mechanism is well known, for more detail, see, e.g., [8]. Despite the heat treatment, the material is transformed exactly at the preliminarily irradiated sites. Photosensitive additives, such as Au, Ag, Cu, are introduced, together with photosensitizers, into the composition of photosensitive glasses. In the presence of platinum-group elements (Pt, Re, Pd, Os, Ir), there is no need in photosensitizers [40].

This feature enables a 2D or 3D microstructuring of photosensitive glasses by photolithography and chemical etching. In photosensitive glass-ceramics fabricated from photosensitive glasses, nontransparent white or colored 3D images can be formed.

The different solubilities of the crystalline and transparent glassy phases furnish an opportunity to form protruding images and manufacture technical products from photosensitive glass-ceramics with a matrix of precisely produced openings with any profiles. The physical and chemical properties that can be controlled by photoexcitation include the optical transmission, microhardness of a material, and its resistance to chemical etching.

Laser technologies are highly attractive from the standpoint of flexibility and production speed, along with the high integration level of each micro-part [43-46]. Photosensitive glasses, such as Foturan™, are of some interest for manufacture of Micro Total Analysis Systems (μTAS)-devices because of their being photosensitive by definition, and, consequently, there being no demand for coating with a photoresist for structuring purposes [35,47].

Foturan™ is an alkali-aluminosilicate glass that consists primarily of silica (75-85 wt % SiO_2), along with various stabilizing oxide admixtures, such as Li_2O (7-11 wt %), K_2O and Al_2O_3 (3-6 wt %), Na_2O (1-2 wt %), ZnO (< 2 wt %), and Sb_2O_3 (0.2-0.4 wt %) [58]. Trivalent cerium (Ce_2O_3) is the photosensitizer, and silver (Ag_2O_3) serves as the nucleation agent.

Thanks to the above-mentioned advantages, glasses and glass-ceramics find application in numerous areas, such as the aerospace instrument-making industry [48], optics and photonics [49], biology and biochemistry [35], computer technologies [50], etc.

Another material used for direct manufacturing of microstructures is fused silica [51-53]. However, it has a substantially poorer efficiency and lower throughput capacity in machining in comparison with such a PG as Foturan™ [54]. Other advantage of PG over fused silica is the possibility of an additional heat treatment for reducing the surface roughness of the microstructures obtained [2]. The possibility of direct fabrication of microstructures in Foturan™ by means of laser irradiation, together with its high-temperature stability, corrosion resistance, and optical transparence, made Foturan™ especially attractive as a material for development of bioanalytical microsystems [35, 55-57].

The main component sensitive to UV light is a rare earth compound, cerium oxide Ce_2O_3. Other compounds of those mentioned above can promote UV absorption, but only at higher concentrations. Cerium has two valence states (3^+ and 4^+), and, also being a reducing agent, it is sensitive to UV radiation and donates a photoexcited electron [59].

The properties of the Foturan™ material are listed in Table 1.

Table 1. Properties of the Foturan™ material [60].

Property	Vitreous state	Crystalline state
Young' Modulus (Gpa)	78	88
Poissons's Ratio	0.22	0.19
Hardness Knoop (Mpa)	4600	5200
Modulus–rupture (Mpa)	60	150
Density (g/cm^3)	2.37	2.41
Thermal expansion @ 20÷300 °C (10^{-6} K^{-1})	8.6	10.5
Thermal conductivity @ 20 °C (Wm^{-1} K^{-1})	1.35	2.73
Transformation temperature (°C)	465	
Water durability DIN/ISO 719 ((μg)Na$_2$O/g)	468	1300
Acid durability DIN 12116 (mg dm^{-2})	0.4	0.9
Porosity (gas–water)	0	0
Electrical conductivity @ 25 °C (Ohms^{-1} cm^{-1}) @ 200 °C (Ohms^{-1} cm^{-1})	 8.1×10^{12} 1.3×10^7	 5.6×10^{16} 4.3×10^7
Dielectric constant @ 1 MHz, 20 °C	6.5	5.7
Loss factor tan(δ) @ 1 MHz, 20 °C	65	25

2.2 Physical fundamentals of the laser processing of glass-ceramics materials

Any change of the optical and other properties of materials is a function of the power density (maximum temperature) in the focal region. It is possible to distinguish modification stages of a material. For example, the optical properties of an insulator may change without any mechanical damage due to a rise in temperature. Also, this change may result from a phase transition (the transition from the crystalline to an amorphous state in silicon leads to a change in the refractive index). Recently, a great deal of attention has been focused on photoinitiated effects in chalcogenide glasses [1, 61-66]. For example, there is a photochemical process in chalcogenide glasses that changes the initial structure of a material, with the resulting change in the bandgap width and refractive index. This photoinitiated process being reversible, it may be of use in a read/write optical memory and in data storage.

Transparent insulators possess a number of characteristic features. First, they have a wide bandgap (> 3 eV, e.g., up to 8.8 eV for sapphire), which provides their transparency in the visible and near-IR spectral ranges at low laser light intensity. For this spectral range, it is necessary to use either laser sources whose wavelength falls within the absorbing region of a material or ultrashort laser pulses to obtain a strong nonlinear response so as to cause changes in a material under the action of moderate-power pulses. In the case of wide-bandgap materials, femtosecond or picosecond lasers can be used to provide local absorption of photons in the transparent medium and enable 3D microfabrication. The size of areas in which structural changes occur may be on the order of the focal volume or even less [67].

The second feature of insulators is their rather low thermal conductivity with a thermal diffusion coefficient on the order of 10^{-3} cm^2/s (for comparison, this value for metals is in the order of several cm^2/s). Therefore, micrometer-size regions will cool in a time of about 10 μs (t ~ l^2/D ~ 10^{-5} s, where l is the size of a region, and D is the temperature conductivity coefficient). Consequently, the effect of several successive laser pulses focused into the same point of the insulator will accumulate if the time between the pulses is shorter than the cooling time. Thus, if a single-shot energy is insufficient for producing any change in a material, modification can be achieved at a high pulse repetition rate due to the energy accumulation effect. The local rise in temperature, caused by energy accumulation, is in progress until the balance between the energy input from the laser and the thermal conductivity action is attained, which commonly occurs after several thousand pulses at repetition rates in the range 10÷100 MHz [68].

A material is ionized when femtosecond laser pulses are focused into a transparent medium. A single photon energy at λ = 800 nm (~1.55 eV) is not sufficient for ionization of a wide-bandgap material. Since the light

intensity in the focal point is sufficiently high ($\sim 10^{14}$ W/cm^2), multiphoton ionization processes are dominant. The femtosecond pulse duration being shorter than the characteristic time of the electron-phonon interaction (picoseconds), it is basically recognized that the photoinduced reaction generated by a single femtosecond laser pulse is a non-thermal process [69]. Consequently, laser radiation acts as a point source of heat in the bulk of the material, and the morphology of resulting structural changes is governed by heat effects [70]. The effect of heat accumulation appears in different ways, depending on the interval of time between successive laser pulses, i.e., on the pulse-repetition rate (Fig. 1).
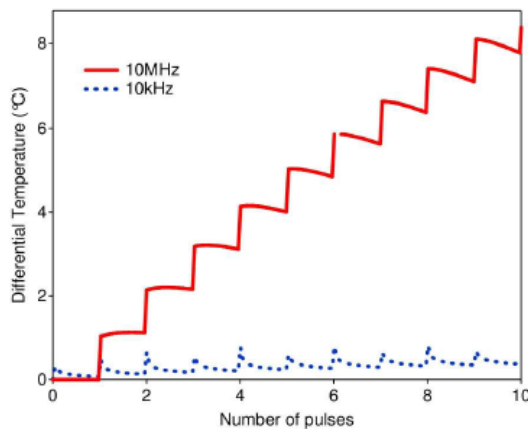
Fig. 1. Temperature versus the number of pulses. Comparison between the 10 kHz and 10 MHz repetition rate s illustrates the cumulative effects of the high repetition rate [69].

If the area of structural changes is sufficiently small ($<< \mu m^3$ in volume), it can be used as a binary unit for a high-density 3D optical memory.

In general, the refractivity grows with increasing laser light intensity [72] or exposure time [73] up to a saturation value. However, such an approach leads to an increase in the area of the modified region, and, therefore, to a poorer spatial resolution and stronger roughness, which enhances the light scattering.

A number of research teams have studied the photophysical processes in PGs exposed to ultrashort laser pulses and their application. Almost the whole amount of research has been concerned with Foturan™; less data are available for a similar glass produced by Hoya (PEG 3). The photosensitive materials containing Ce^{3+}, whose absorption peak lies at 314.5 nm (3.94 eV, FWHM $\sim$ 0.5 eV), have been irradiated with nanosecond laser pulses at wavelengths of 193 nm (6.42 eV) [72], 248 nm (5.0 eV) [75], 266 nm (4.66 eV) [74], and 355 nm (3.49 eV) [75, 76], and also with femtosecond lasers at wavelengths of 775 nm (1.6 eV) [7], 800 nm (1.55 eV) [77], and 1027 nm (0.03 eV) [78]. It follows from the above data that there are other sources of photoelectrons, which can boost the exposure, or there are multiphoton absorption processes. There are processes of both kinds in Foturan™. Using a femtosecod laser, it was demonstrated [7] that, to stimulate formation of a crystal phase in

Foturan™, the irradiation must be accompanied by a 6-photon absorption at the wavelength of 775 nm. Experiments with nanosecond lasers, carried out at the Aerospace Corporation, demonstrated that, for both the wavelengths of 266 nm and 355 nm, the threshold exposure necessary for an etchable crystalline phase to be formed strongly depends on the power density [79] and this dependence was found to be quadratic in [80].

The role of cerium as the source of electrons was studied in [81, 82] on Foturan™ samples containing cerium (c-Foturan) and free of cerium (nc-Foturan). The efficiency of Ce^{3+} in generation of photoelectrons was measured at two laser light wavelengths ($\lambda = 266$ nm and $\lambda = 355$ nm), which lie below and above the peak of the absorption band of the photosensitizer (Fig. 2).
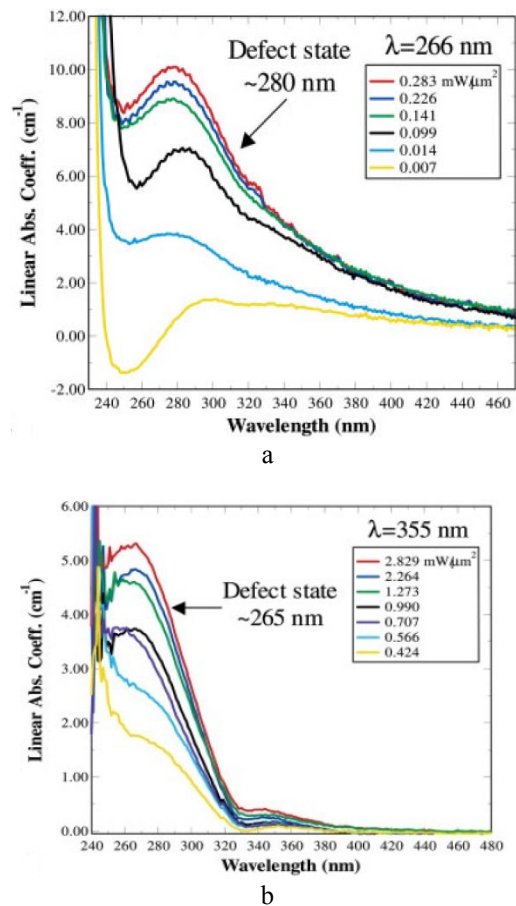

a

b

Fig. 2. Optical transmission spectra measured at different incident laser light intensities for λ = 266 nm (a) and 355 nm (b). The intensity of the spectra corresponds to the state with a latent image (exposed state) and is determined by the ratio of its intensities for the exposed and unexposed states [81, 82].

The optical transmission spectra shown in Fig. 3 correspond to the state with a latent image and demonstrate the influence of cerium on the impurity levels (defect states) excited by laser radiation. A suggestion that cerium may play a minor role as a donor of photoelectrons in processing of photosensitive glass ceramic materials at $\lambda = 266$ nm was made [82].
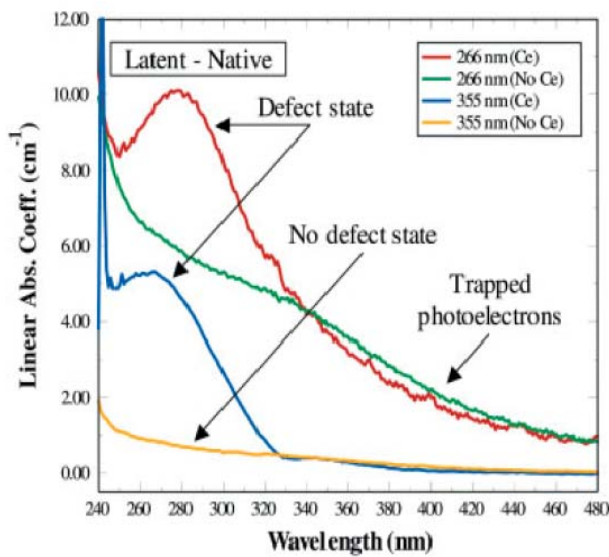
Fig. 3. Optical transmission spectra for c-Foturan and nc-Foturan samples following laser irradiation at λ = 266 nm and 355 nm. The incident laser light intensities were 0.283 mW/mm² and 2.829 mW/mm² for λ = 266 nm and 355 nm, respectively [82].

In [3], the mechanism of the photoresponse of a photosensitive glass to pulses of light from a femtosecond IR laser was studied, and the electron excitation process was examined by determining the critical dose and the change of the optical-absorption spectrum upon irradiation with the femtosecond laser. In addition, the photoreaction mechanism was discussed in comparison with the case of an irradiation with a nanosecond UV laser (Fig. 4).
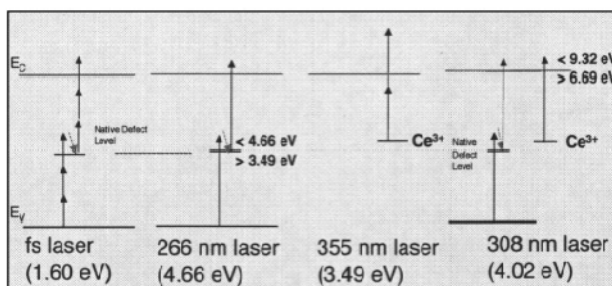

Fig. 4. Free-electron generation processes in a photosensitive glass by different lasers [3].

The dependence of 3D crystallized areas formed in the bulk of a photosensitive glass (Foturan™) by focused femtosecond laser pulses and subsequent heat treatment on the laser power density was analyzed in [83] by means of scanning electron microscopy.

The photoinitiated process (formation of a latent image and its subsequent development and fixing) occurs in several well-known stages (for an example, see [84]).
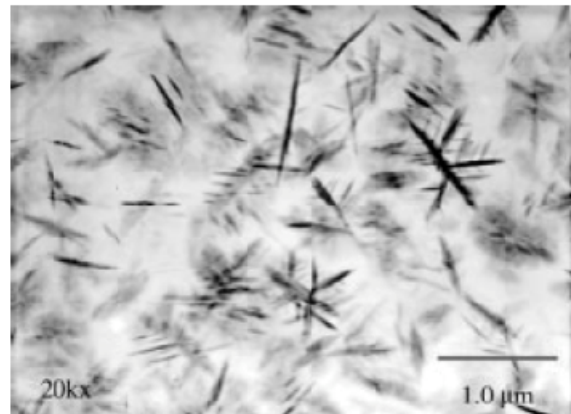

Fig. 5. TEM image of Foturan irradiated with a UV laser thermally processed. The dendritic morphology of lithium metasilicate crystals is shown after a chemical etching [8].

The lithium metasilicate (LMS) phase is dissolved in dilute hydrofluoric acid (HF) [85], and, upon an appropriate heat treatment, the ratio between the etching rates of irradiated and unirradiated areas approaches 50 for some photosensitive glass-ceramics [40]. Such a large difference between the etching rates can be attributed to the lower resistance of crystalline LMS particles to HF in comparison with the residual glass.

Elements with high spatial resolution can be obtained by using the etching-rate difference between an initial glass and a polycrystalline material. The processing stages of photosensitive glasses include [58]:

1. Exposure of a basic material to a UV lamp with high-intensity emission in the range from 300 to 350 nm through masks providing irradiation of only required regions on the glass surface.

2. Heat treatment under certain temperature conditions.

3. Chemical etching in dilute (5-10 wt %) HF.

If the heat treatment is performed at a temperature below the crystallization point, the refractive index of the material changes upon selective precipitation of silver nanoparticles through a photochemical reaction. The theoretical limit of the spatial resolution is determined by the size of silver nanoparticles. Depending on the concentration of the silver dopant in the glass and on the heat treatment conditions, this size is on the order of tens to a hundred of nanometers, and the following mechanism is operative [75]: a free electron generated by opening of an oxygen bond remains after exposure near the defective center and serves as a center for formation of silver nanoparticles. In this case, the diffusion of silver during the heat treatment is not arbitrary, but occurs under control of Coulomb forces in the direction of the exposed area. It should also be mentioned that precipitation of silver nanoparticles in the glass under a femtosecond treatment may occur in the optical breakdown conditions (local melting followed by rapid cooling) due to the high radiation intensity [86]. Then the variation of refractivity is a thermally induced process. In this situation, the spatial resolution is governed not only by the area of multiphoton absorption, but also by that of heat transmission. In the

first case, the laser radiation intensity is a threshold parameter for multiphoton absorption processes and is well below the intensity necessary for a direct change in the refractivity upon an optical breakdown in a material [7].

One more way for modification of photosensitive materials via a controllable phase transformation is by using CO_2-laser radiation with a wavelength of 10.6 μm. The laser-induced amorphization (decrystallization) of glass ceramics was studied by means of optical pyrometry and video recording in [10] and the ranges of power density and exposure to the 10.6 μm light, required for amorphization of a typical glass ceramic, $SiO_2 \cdot Al_2O_3 \cdot CaO \cdot MgO \cdot TiO_2$ (Pyroceram ST-50-1), were determined (a power density is about $5 \cdot 10^5$ W/m^2). The resulting high-temperature structure is frozen in the amorphization mode upon laser irradiation due to the relatively high cooling rate $V_c = 50 \div 100$ K s^{-1}, which is provided by the heat conduction mechanism in the glass ceramics. The amorphous phase obtained can be recrystallized by repeated irradiation at a lower power density 10^5 W/m^2 (and, therefore, at lower heating and cooling rates), which enables its reverse (secondary) crystallization [87]. Specific features of these processes were studied in [11] and interpreted in terms of the thermophysical kinetics and a novel concept of amorphous materials as vacancy-distorted crystals. The rapid laser crystallization of amorphous (glassy) materials can only be explained by taking into account the key features of their behavior in a nonequilibrium state. To adequately account

for this process, it is necessary to assume that the melt resulting from rapid laser heating contains residual quasi-ordered polycrystalline structures, which play a key role in the crystallization process. These experiments demonstrated that the IR CO_2-laser radiation can be used for local control over the structure and properties of other silicate glasses and glass-ceramics. This was demonstrated for a glass sample of lithium disilicate $Li_2O \cdot 2SiO_2$ in [88], for Ti-containing glasses in [89], and for PGs in [90].

There is a phenomenon to be mentioned separately, known as optical bleaching waves generated by continuous-wave Nd:YAG laser radiation in glass-ceramics [91]. Changes in the transparency and temperature of ST-50-1 glass-ceramic during exposure to a Nd:YAG laser was studied (Fig. 6). The crystalline phase absorbs radiation at 1.06 μm, while the melted phase is transparent in this energy range. As a result, the absorbing zone is shifted to the front of bleaching. In addition, the occurrence of the feedback between the heating rate and the optical properties results in the development of complex kinetics of both the temperature distribution and optical properties. This specific thermooptical effect leads to the appearance of waves of optical bleaching. A mathematical model of these periodic oscillations of the transparency and phase-structure has been suggested [92]. The principal features of the process are determined by the nonlinear nature of heating due to the existence of a feedback between the optical and thermal characteristics of glass-ceramics: light absorption and temperature.
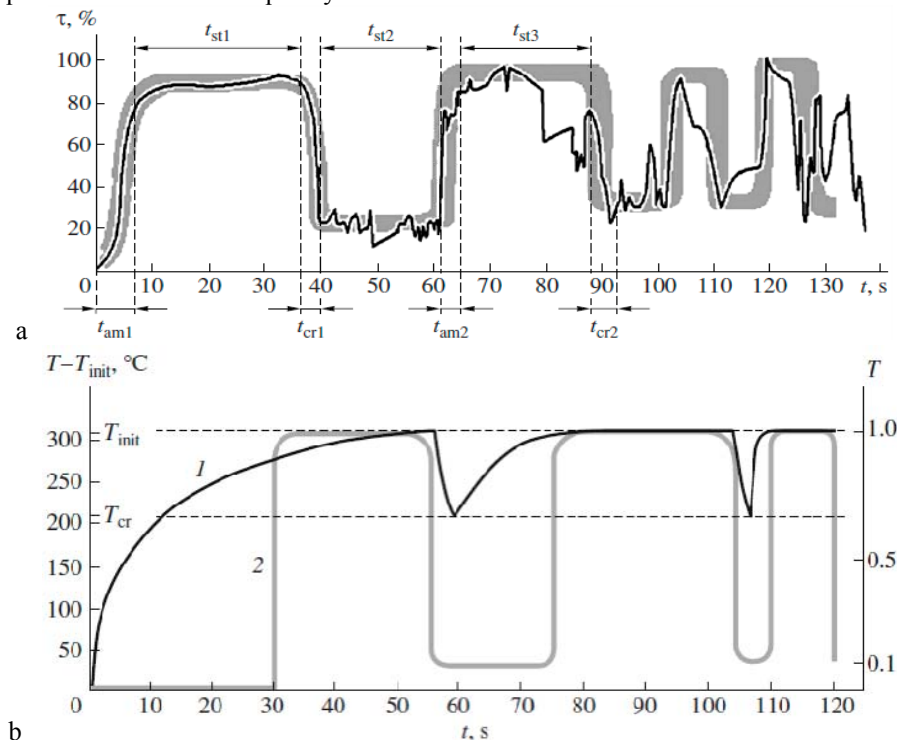

Fig. 6. *a) Transparency τ of a glass-ceramic plate vs. duration t of exposure to continuous-wave Nd:YAG laser radiation [91]; b) Results of model calculations for a 0.6-mm-thick ST-50-1 plate . (1) width-average temperature T at the center of the illuminated area; (2) corresponding qualitative time - dependence of the plate transparency τ [92].*

Finally, it can be stated that inhomogeneous and unsteady temperature fields arise in the substance under

laser irradiation leading to phase transitions that can enable conversion of the initially "passive" material to the

"creative" state. Careful selection of laser processing parameters, such as wavelength, pulse width, focusing and power density control in time and space, could open a way for development of deep-seated integrated devices that could be designated as truly nano- or microdevices. The next part of the paper gives a brief review of such devices and ways for their production.

2.3 Applications to development of multifunctional elements

One of modern methods for fabrication of various microstructures on the surface and in the bulk of glass-ceramics and glasses is by laser exposure of the substrate material. In particular, the present practical interest in the laser processing of photosensitive glass-ceramics is due to the advanced features of various devices based on this technology.

The laser micromachining is now one of the main methods for fabrication of various kinds of microdevices and microsystems.

There are some areas of laser processing of glassy materials:

- development of various transparent microoptical components on the surface of nontransparent glass-ceramics;

- structural modification of PGs, which includes formation of 3D structures in the bulk of a material.

The aforementioned processes of local laser processing of glasses and glass-ceramics have been intensively studied recently, with great attention given to the structural modification.

There are several approaches to development of 3D microstructures. The laser is a very convenient tool for 3D micro- and nanomachining because laser light is suitable for various kinds of treatments, which can be divided into two types. The first is by removal of regions exposed to laser light. This category includes etching, engraving, ablation machining, and lithography. The second is based on retaining the exposed areas. Phase-structural modifications belong to this type. Laser micromachining has a number of advantages over such techniques as mechanical processing, micromachining by a focused ion beam [93] and electron-beam treatment [94, 95]:

- processing of various kinds of materials is possible, from soft, such as polymers and biological tissues, to hard materials, such as glass and even diamond;

- the processing rate substantially exceeds that of the conventional methods;

- internal modification and micromachining of transparent materials is possible via multiphoton absorption of ultrashort laser pulses. This process is only possible in laser processing;

- processing of systems of various scales, from macro to micro or even to nano, is possible;

- there is no need for special processing conditions, such as vacuum or a protective gas.

Direct laser-induced modification by exposure to femtosecond lasers is used to obtain structural changes in transparent materials, such as glasses, crystalline materials, and polymers. These materials can be, and are already used for development of various devices and technologies, such as photonics [26], waveguides [52, 96-

101], optical information storage [102-104], local polymerization [105], beam splitters [106-109], couplers [110-114], diffraction gratings [115-120], optical amplifiers [121-123], Fresnel zone plates [124], and generation of multicolor images [125]. An extensive review of the femtosecond laser direct-write technique as a technology capable of producing optical waveguide devices within the bulk of transparent materials without need for lithography, etching, controlled environment, or laborious sample preparation is given in [126].

2.3.1. MEMS, MOEMS

A technique for processing of photosensitive glass-ceramic materials, which combines the advantages of the serial and batch processing has been developed by the Aerospace Corporation [8, 127-129]. It was based on the fact that the etching depth in a material can be controlled by the number of laser pulses during the irradiation. In other words, there is a strong correlation between the etch rate ratio (for the untreated and exposed materials) and the laser power density (Fig. 7). Therefore, it is possible to precisely control the dimension ratio of the microelements formed during the laser machining.
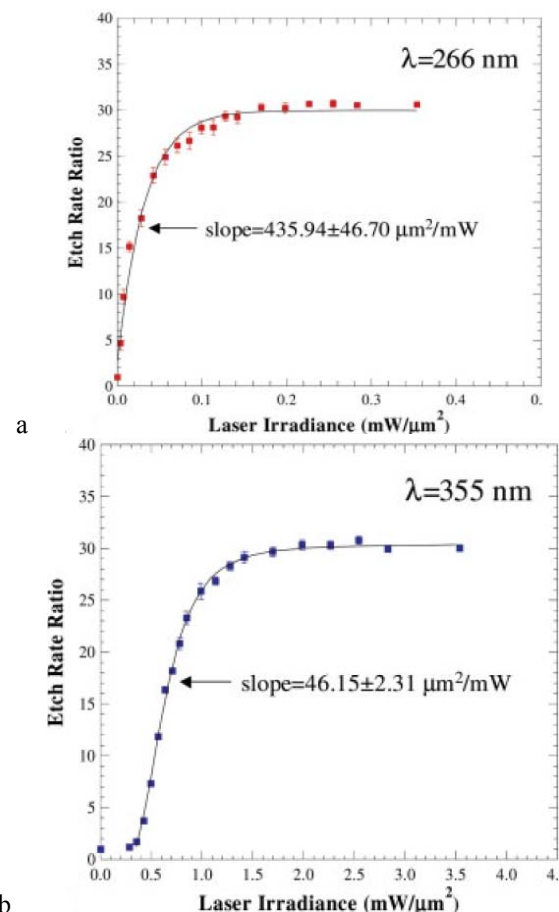
a

b

Fig. 7. Measured etch-rate ratios as a function of the incident laser irradiance at $\lambda = 266\,nm$ (a) and $\lambda = 355\,nm$ (b). The solid squares correspond to the measured etch-rate results and the solid lines represent the optimized Hill equation fits to the experimental data [129].

It was also shown that, by appropriate control over the laser exposure, it is possible to produce local changes in color and absorptivity in the visible and IR spectral ranges (Fig. 8).
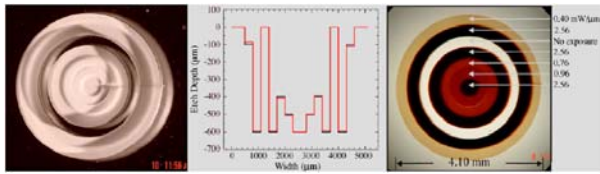

Fig. 8. Structures fabricated by the direct-write variable-dose laser technique. Left: chemically etched microfabricated structure. Middle: measured depth profile of the structure, along with the design requirements. Right: controlled local optical transmission change in the photosensitive glass-ceramic material [129].

Some examples of elements fabricated by this technique are shown in Fig. 9. This method can produce various parts of MEMS and MOEMS with high precision, without use of masks and multistage treatments.
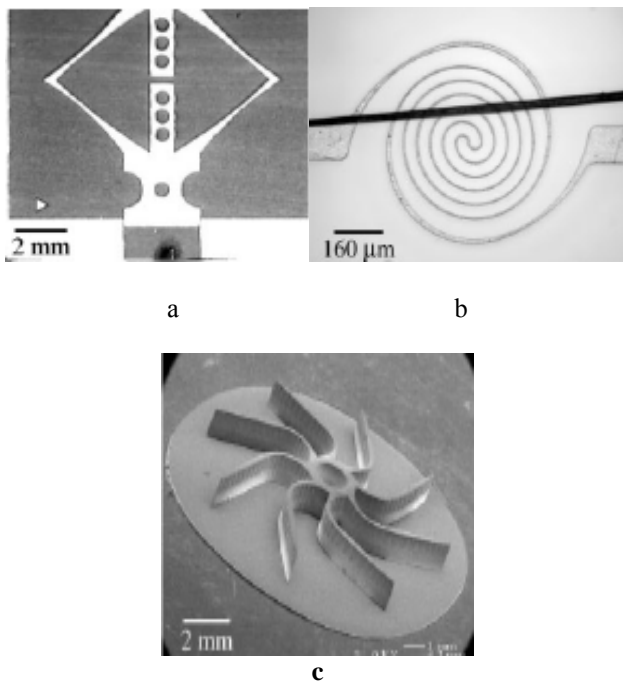

a   b

c

Fig. 9. Optical micrographs of several compliant structures fabricated with Foturan™. A wishbone spring (a), a hotplate coil spring with a human hair overlaid for visual reference (b), and a microscopic rotary turbine blade (c) [8].

In general, the surface roughness of a material being processed can be adjusted in several ways. The first of these is by changing the thermal treatment protocol [8]; an alternative way to smooth the surface roughness is by annealing the processed part after the chemical etching [130] or by a photolytic treatment. Also, a post-etch

annealing can be used to join multiple structures to create optically transparent 3D devices [131].

Previously, mercury lamps [33, 132] were used for processing of photosensitive glasses. This method could generate only superficial microstructures. Later, another processing technique was developed, based on nanosecond pulses of UV lasers, followed by heat treatment and chemical etching [80, 127]. This method enabled fabrication of a multitude of highly versatile 3D structures (microfluidic, microelectromechanical, and optoelectronic systems) (see, e.g., [133-135]). At the same time, the depth of the structures obtained is less than 1500 μm, i.e., they are situated not far from the surface [75] due to the resonant absorption of UV radiation by a material.

To avoid these limitations, lasers whose emission wavelength is not resonant for a material are used, for example, femtosecond lasers for irradiation of photosensitive glasses at 400 and 800 nm [72, 54]. This enables fabrication of deeply buried 3D microstructures without modification of the surface.

The commercial development of the methods mentioned above is described in [136]. An application of direct laser structuring for fabrication of scalable 3D microstructures (masks, sensors, parts of complicated machines) with low development costs and manufacture with a short production run were demonstrated.

A process employing non-ablative 3D laser patterning of photo-structurable glass-ceramic substrates for manufacture of microsystems and components used in MOEMS and MEMS applications was presented in [137].

2.3.2. Microfluidic and biomedical applications

The growing demand for microdevices having high efficiency and data-output rate for biochemical analyses and medical monitoring stimulates development of 3D technologies for production and binding of versatile microelements into a single chip. The design of "all-in-one" (lab-on-chip) microchips in which different (liquid, mechanical and optical) components are formed on a common substrate is still a complicated task, starting from the development stage and finishing with that of mass production [138]. The development of a technique for manufacture of 3D hollow microstructures embedded in materials made it possible to improve the production of microanalytical systems in chemical analyses.

A great progress in the integration of optical and liquid systems has been achieved in recent years, which considerably improved the functionality of "all-in-one" microchips. Fluidic microdevices with integrated optical structures, such as optical waveguides [139-141], micro-optical gratings [142-144], optical fibers [145], microoptical mirrors [7, 146], and micro-optical cylindrical lenses [147] have been fabricated.

Glass-based opto-fluidic devices integrating microchannels and optical waveguides have been fabricated by femtosecond laser pulses and subsequent wet etching in [148]. Use of microchannels with a neck diameter slightly smaller than the cell size enables sharp, constant, and unambiguous cell detection by transmission

and reflection, as well as cell processing by coupling of laser radiation.

It is possible to say that the origination of microfluidic systems based on a single plate, or μTAS-systems, made the same revolution as the development of transistors and integrated circuits in electronics [149]. The recent trends in application of polymeric materials for manufacturing of microdevices [150, 151] are attributable to the fact that they are less expensive and more suitable for mass production in comparison with siliceous materials. However, the problem of incompatibility of materials still remains important since polymeric channels, valves, and pumps show a tendency to react with organic solvents, thereby causing pollution and failure of devices [151]. Therefore, systems based on siliceous materials are preferable when chemically active substances are to be handled.

At present, microfluidic devices are mostly produced by photolithography with direct laser exposure [153, 154], hot stamping [155], imprinting (transfer of a necessary profile by pressure) [156], or injection molding [157, 158]. These manufacturing methods are well proven and suitable for mass production of microfluidic systems based on polymeric materials. At the same time, all of them demand gross expenditure of time and finance because adjustment, bonding, and assembling of separate microcomponents are required [159].

The appropriate 3D micromachining enables development of complicated micromechanical devices, including mobile objects within glass. For example, a dye laser was produced by agglomeration of microfluidic and microoptical parts in a single glass chip. The laser operated on Rh6G dye injected into glass through a microchannel, four hollow microplates integrated with microfluidic elements served as mirrors of the laser cavity [130]. It can be seen, for example, in [55], where it was shown that localized and deeply buried structures can be potentially formed through multiphoton excitation processes and nonlinear self-focusing effects (Fig. 10). A similar U-shaped structure has been fabricated in Foturan™ [160] and silica [161].

Using an astigmatically shaped beam, microchannels with a circular cross section and a length of up to 1.5 mm were produced in [162]. It should be mentioned that microfluidic channels and optical waveguides in 3D configurations can commonly be integrated on a single substrate by the same laser source with different irradiation parameters. Also, to obtain high-accuracy structures within a transparent material, it is necessary to take into account spherical aberrations and self-focusing phenomena in the case of ultrashort laser pulses [163].

In [164], vertical micro-holes with a circular cross-section and clear edge were fabricated within Foturan™ by femtosecond laser writing followed by heat treatment and chemical etching. Previously, 3D microdrilling of photomachinable glass by the multiphoton process with 400-nm laser pulses and subsequent heat treatment and chemical etching has been reported [165].
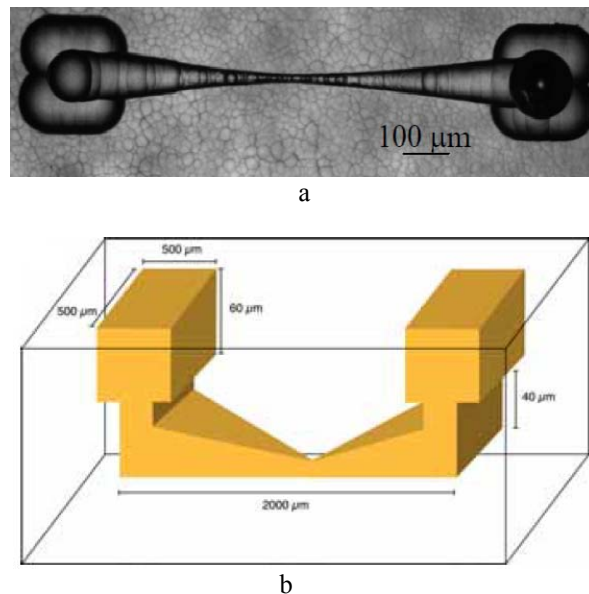

Fig. 10. (a) Top View of a U-shape channel embedded 100 μm below the surface (b) 3-D sketch of a microsystem for observation of bacteria [55].

A compact and highly integrated interferometric device was demonstrated in [166]. This device enables sensing of the refractive index of the content of a microfluidic channel.

A 266 nm laser with a high pulse repetition rate and a very low power (several tens of mW) was employed in laser-induced backside wet etching (LIBWE) for machining of Borofloat 33 glass in [163].Various effective etching chemicals for the LIBWE process were also examined in order to understand the etching mechanism.

2.3.3. Photonic applications

The variation of the refractivity within glass and the generation of an array of modified nanodots by a femtosecond laser were shown in [167]. The refractive index is changed at modified points by a factor of 10^{-2}, which is sufficient for use in 3D optical memory with ultra high density. The possibility of fabricating 3D optical waveguides embedded in glass by femtosecond laser scanning was also shown in [52]. Raising the energy of a femtosecond laser energy leads to formation of microcavities within glass, instead of changing the refractive index. Initially, a single void appears at the focusing point and, due to the sample displacement, a regular array of voids is formed [168]. A regular array can be spontaneously formed along the radiation propagation direction at distances of several micrometers as a result of focusing of a single femtosecond beam [169]. In [169-171], the effect of various laser treatment characteristics, including power density, number of pulses, and focal depth, on the shape and period of the voids array was studied. In photonic devices, such a regular array of voids can be used, for example, for light beam collimation or can serve as the wave filter [170].

Another approach is to use microgratings produced within soda–lime glass by two-beam interference of a single 130 fs laser pulse at a wavelength of 800 nm [144]. If one recording beam is modulated as a signal beam, optical information can be stored in transparent materials by this holographic method.

Also, writing of 3D dots within glass may become a useful method for fabrication of optical memory with both an ultra-high storage density and an ultra-high recording speed. The contrast between the irradiated and unirradiated parts grows with increasing average laser light power and irradiation duration [104].

The possibility of 3D optical data storage within a specific zinc phosphate glass containing silver by third-harmonic generation (THG) imaging was demonstrated in [103]. Information is stored within glass via femtosecond laser irradiation below the refractive index modification threshold. The same laser is used for the THG readout.

So-called phase-change memory alloys widely used in re-writable optical discs such as DVD-RAM are discussed below in this review.

Since glass-ceramics are commonly unsuitable materials for fabrication of optical components due to the strong scattering at optical wavelengths, amorphization of glass ceramics could enable such possible and tested applications as arrays of microlenses [175], optical windows, non-spherical lenses [176], planar waveguides [177], integrated diaphragms, optical recording in glass-ceramic and Ti-containing glass films [9], complex-integrated micro-optical components, or just new optical micromaterials with unusual refractive index (amorphized Al_2O_3) and spectral properties.

An extensive study of the refractive index modification by femtosecond laser light in a wide variety of multicomponent borosilicate, aluminum–silicate, and heavy-metal oxide glasses, along with lanthanum–borate and sodium–phosphate glasses, was reported in [172].

Another interesting example of implementation of the given technology is the formation of a buried waveguide for visible and IR spectral ranges in Foturan™ with a femtosecond laser (Fig. 11). The waveguides were fabricated by exposure of the parent glass to 135-fs laser pulses at a wavelength of 775 nm and pulse repetition rate of 1 kHz [173]. The samples were scanned in the direction normal to the laser polarization direction, at a speed of 50 to 200 mm/s and power density in the range 5÷36 J/cm². After that the samples were heat-treated for 6 h at a temperature of 520ºC.

Another way to use the technology based on CO_2-laser-induced change of properties of glass-ceramic materials is to fabricate various microoptical elements, such as lenses and lens arrays, waveguides and other waveguiding components, diffraction gratings, integrated diaphragms, etc. [178]. The change in the refractive index and surface profile has been used as the first step for fabrication of optical elements. The second stage consisted in chemical processing, including the ion-exchange technique and etching of irradiated and unirradiated areas. A similar technique was developed for Corning 7059 glass in [179], with convex microlenses obtained.
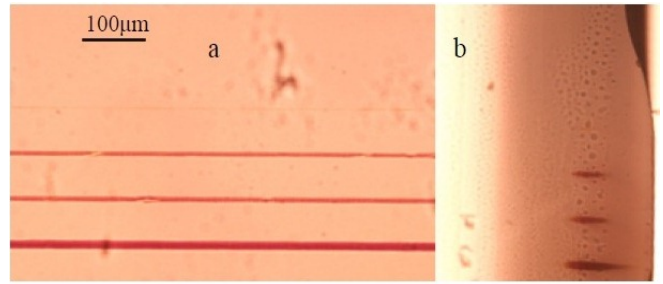

Fig. 11. Microscopic view under backlight illumination of the side (a) and end-section (b) of waveguides formed at 200 mm/s. Waveguides were written at energy densities 12.6, 14.4, 18 and 36 J/cm², from top to bottom of a picture, correspondingly [174].

For comparison, the fabrication of rod-like and spherical silica microlenses by CO_2-laser melting was reported in [180], and that of fused silica and microlenses, microlens arrays, and diffraction gratings on a polyethylene substrate, in [181].

The encoding of hologram gratings and crossed gratings within photo-insensitive transparent materials was examined in [182] by using a chirped pulse from a mode-locked femtosecond pulsed laser. This technique offers a method for fabrication of embedded grating structures that can be used in fiber gratings, planar optical waveguides, distributed-feedback lasers, and multilayered optical memories.

A new method for fabrication of internal diffraction gratings by modification of the bulk refractive index was demonstrated in [183] for planar silica plates, with low-density plasma formed by a tightly focused femtosecond laser. The modification of the refractive index with low-density plasma could be a useful technique for fabrication of optical transmission diffraction gratings for such applications as optical sensors and optical communications.

The diffraction efficiencies of holographic gratings obtained in two photosensitive glasses, Foturan™ and PEG3, were compared in [184].

High-efficiency (absolute diffraction efficiency exceeding 96%) Bragg gratings were fabricated in sodium-zinc-aluminum-silicate glass doped with cerium, silver and fluorine by exposure to UV radiation and subsequent thermal development [185]. Phase-volume holograms recorded on photo-thermo-refractive glasses are described in more detail in [186].

The direct laser writing technique producing subwavelength nanostructures irrespective of the experimental limiting factors was reported in [70]. A universal mechanism could be used for various ion-doped matrices (glass, polymer), in which the reduction process and the thermal diffusion are involved thanks to the high repetition rate of the femtosecond laser (Fig. 12).
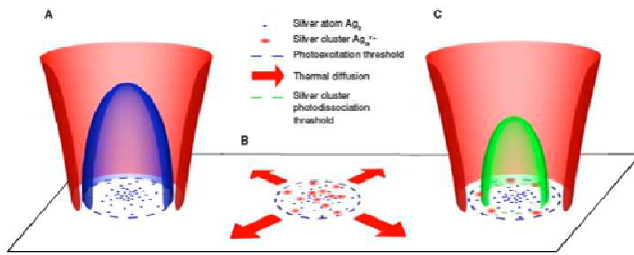
Fig. 12. Schematic of how nanostructures are formed. (A) Photoelectrons released under laser irradiation are trapped by Ag^+ ions to form silver atoms Ag^0 represented by the blue spots. The Ag^0 atoms are distributed over the interaction area delimited by the blue dashed circle. This area is smaller than the laser beam size because of the nature of the nonlinear interaction. (B) After 1000 pulses, the local temperature increases and diffusion occurs, as illustrated by the red arrows. Ag^0 and Ag^+ interact to give silver clusters Ag_m^{x+} with $m<10$, illustrated by the red spots. (C) Subsequent laser pulses cause photo-dissociation of the newly formed Ag_m^{x+}, except on the edges of the interaction area, leaving a cylindrical nanostructure composed of silver clusters. The photo-dissociation threshold of the silver clusters is represented by the green dotted circle [71].

These illustrations clearly show that the laser-induced modification of the properties of glass-ceramic materials is a significant and topical issue of the present-day research. It seems that there are two advanced applications of the given technology. The first is the development of a new type of optical memory with extra high-density of data recording. The second consists in manufacture of versatile microdevices that are capable of operating under severe conditions, have low production cost, and strong

variability in generation of surface and bulk configurations.

3. Chalcogenide phase-change memory alloys

3.1 What are phase-change memory alloys?

This section of the review deals with Te-based materials, often called phase-change memory alloys. The idea to use an amorphous-to-crystal phase transition to record information has been suggested by S.R. Ovshinsky in the mid 1960s in his seminal paper titled "Reversible electrical switching phenomena in disordered structures" [187] and is based on an assumption that optical and electrical properties of the crystalline and amorphous phases have a pronounced contrast.

It should be noted, however, that while the above assumption is usually correct for electrical properties, for optical properties this is not always the case. The electrical contrast is primarily determined by differences in the carrier mobility which decreases drastically upon amorphisation. At the same time, optical contrast is determined by the density of states in the two phases and the transition matrix element. For most covalently bonded semiconductors both the density of states and the matrix element are similar, resulting in rather similar optical properties. Phase-change alloys are an exception from this rule and exhibit a pronounced optical contrast between the two phases which makes them suitable for memory applications. A comparison of a change in optical properties upon crystallisation between non-phase-change materials and phase-change materials is shown in Fig. 13.
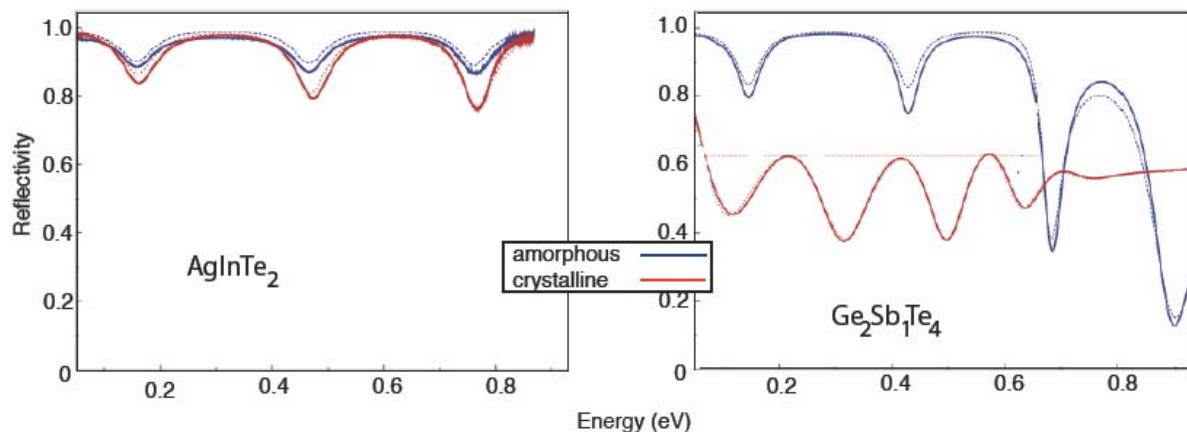

Fig. 13. Reflectivity difference between amorphous and crystalline phases for a non-phase-change material, (left) and phase-change alloy $Ge_2Sb_1Te_4$(right), after [188].

Other requirements for memory applications are high stability of both phases. Currently, the standard stability requirement for consumer applications is 10 years at 160 °C. The high stability should co-exist with a fast switching rate between the two phases. In the case of

phase-change alloys, amorphisation usually takes place on a scale of 1 ns and crystallisation on the scale of 10 ns. The co-existence of high switching rate and high stability is very unusual and makes phase-change alloys exceptional.

It is generally believed that the transformation between the two phase has thermal origin. A short intense laser (or current) pulse heats the material above the melting point, which is followed by fast quenching generating an amorphous phase. A less intense but longer pulse heats the material to the crystallisation temperature and reverses to structure. Recently, there has been accumulating evidence for an important role of electronic excitation in both amorphisation and crystallisation processes [189-191].

In what follows, we start with a description of the reversible crystal-to-amorphous transition and most promising materials used for this purpose. This is followed by the discussion of the structure of the two phases. The section is concluded by a discussion of the mechanism of the phase-change process and the effect of electronic excitation on the phase-change.

A melt can be solidified in two different ways. If the melt is cooled slowly, an equilibrium crystalline phase is formed. If, on the other hand, the melt is cooled fast enough so that the structure cannot follow the change in temperature (typically ca. 10^7 K/s cooling rats are needed to amorphise a phase-change material), the disordered phase is frozen; one obtains a supercooled liquid and subsequently a glass. When the obtained glass is annealed at temperatures between the glass-transition temperature and the melting point, it gradually transforms into the crystalline state. One can thus cycle a material between the ordered (crystalline) and disordered (amorphous) phases. With respect to chalcogenide alloys, the reversible crystal-to-amorphous transformation is called a phase-change process and materials undergoing such changes - usually Te-based alloys - are called phase- change materials.

From the description above it follows that almost any material can be prepared in either crystalline or amorphous phases. While this is generally true, there are several factors that determine practicality of such reversible changes between the ordered and disordered phases.

One of the major parameters is the characteristic time scale. Thus good glass formers possess a very high viscosity and crystallisation of such glasses can take years even at temperatures very close to the glass-transition temperature. Marginal glass formers, on the other hand, can crystallise in nanocesonds.

Another important parameter is cyclability, or the number of crystallisation-amorphisation cycles the material can withstand without degradation of properties. This is predominantly determined by the ability of a material to maintain the same single phase in the crystalline, amorphous, and liquid phases. Materials that are subject to phase separation usually exhibit strong degradation of properties after several cycles. Stresses generated in repeated cycles at crystal-amorphous interfaces due to density difference between the crystalline and amorphous phase is another factor limiting cyclability in device structures

R&D of phase-change optical storage has a long history starting with the discovery of the switching effect in some chalcogenide alloys. In particular, in $Si_{12}Te_{48}As_{30}Ge_{10}$ it was found that application of a voltage that exceeds a critical value called threshold voltage, the chalcogenide alloy switched from the low-conductivity state to the high-conductivity state [187]. When the current in the high-conductivity state was reduced below the characheristic value termed the holding current the unit switched back to the original low-conductivity state. The observed switching process was reversible and could be repeated many times. The observed increase in the conductivity was attributed to the formation of a current filament, growing in diameter with increasing current flow. In the same paper, it was reported that by tuning the composition a memory effect was observed that was attributed to a change in the structure of the material, namely, "after switching from a highly resistive state, structural changes result in the preservation of a conductive state even when the current is totally removed. The material can be reversibly switched back to the highly resistive state by application of a current pulse of either polarity exceeding a threshold value". This finding marked the beginning of intensive - and extensive - research on phase-change materials.

A group of materials, typically (but not exclusively) Te-based alloys, exhibit very high amorphisation and crystallisation rates on the order of nanoseconds which, combined with large cyclability and a pronounced property contrast between the crystalline and amorphous phases, makes them ideal for memory applications. The most studied commercially used materials lie along the quasibinary GeTe-Sb$_2$Te$_3$ tie-line and are usually referred to as GST alloys. In this review we concentrate on Ge-Sb-Te alloys as the most studied and best understood class of phase-change materials.

Since the properties of a material are determined by its structure, knowledge of the details of the average and local structure is of paramount importance for insightful device development.

3.2. Structural studies

3.2.1. Crystalline phase

It is natural to start the description with the binary GeTe which is the simplest material in the GST system. GeTe is a narrow band-gap semiconductor and also a ferroelectric with the simplest conceivable structure containing just two atoms in the primitive cell. In the low-temperature ferroelectric phase GeTe possesses a rhombohedral structure with space group R3m. This structure can be viewed as a rock-salt structure slightly distorted along $< 111 >$ direction with a subsequent shear relaxation along the $< 111 >$ direction. The driving force for the formation of the rhombohedral phase has been a subject of various studies in the past [192]. In this phase, Ge and Te atoms are six-fold coordinated to each other with subsets of three shorter (2.83 Å) and three longer (3.15 Å) bonds often described as a Peierls distortion [193]. While it has been previously argued that the structure changes to cubic at higher temperatures [194], local structure studies using EXAFS and pair-distribution function analysis of total scattering demonstrated that the

local distortions persist across the ferroelectric-to-paraelectric transition [195, 196].

Bragg diffraction studies performed on $Ge_2Sb_2Te_5$ concluded that amorphous films crystallise into the cubic phase. Based on results, the crystal structure of $Ge_2Sb_2Te_5$ was identified as the rocksalt (NaCl) structure [197]. From Rietveld refinement it was concluded that the anion face-centered cubic (fcc) sublattice is fully occupied by Te atoms with Ge and Sb atoms randomly located on the cation sublattice [198, 199]. The stoichiometry of the structure requires that there are vacancies on the Ge/Sb sites and their presence has been confirmed by structure refinement. The proposed structure is shown in Fig. 14. The cubic phase is metastable and transforms into the stable trigonal phase at temperatures above, but the stable phase is not formed during the reversible phase-change process and will not be further discussed here. It was subsequently shown that the rock-salt structure is characteristic of a large range of Ge-Sb-Te alloys [200].
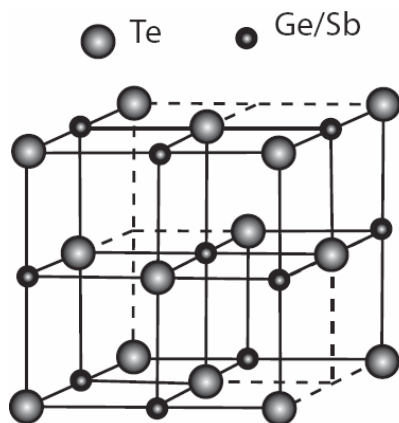

Fig. 14. Structure of the metastable rock-salt phase of Ge-Sb-Te alloys. One fcc sublattice is formed by Te atoms and the other one is formed by Ge and Sb atoms and vacancies.

Subsequent extended X-ray absorption fine structure (EXAFS) studies performed by various groups [201, 202] revealed that the Ge-Te bond length in the metastable GST is ca. 2.83 Å, i.e. significantly shorter than might be expected based on the rock-salt structureas determined by XRD and the obtained lattice parameter of slightly over 6.00 Å. Based on these results, it was argued [202] that the structure of metastable GST225 does not possess the rocksalt symmetry but is locally distorted similar to that of the binary GeTe that possesses a rhombohedral structure (that can be alternatively described as distorted rock-salt structure) with subsets of three shorter and three longer bonds. The distortion of the Ge atom location has been subsequently confirmed experimentally using scattering measurements [203]. The Sb-Te bond length was also found to be shorter than half the lattice parameter (2.94 Å, [202]). It is interesting to note that while the obtained bond lengths are significantly shorter than those expected from the obtained lattice parameter and the rocksalt symmetry, they are at the same time significantly longer that the sum

of the corresponding covalent radii, which suggests that the bonds are not purely covalent.

The rock-salt like arrangement of atoms in the crystalline phase requires the formation of six bonds by each participating atom while at the same time, the number of valence electrons located on Ge and Sb atoms is lower. A way to ensure six bonds is by virtue of sharing the valence electrons among several bonds with less than two electrons per bond on the average through resonance bonding, the best known example of a materials with resonance bonding is benzene.

A similar idea was applied to solids and, in particular, to IV-VI crystals. Lucovsky and White [204] were the first to discuss this possibility and its consequences. In particular, in this work resonance bonding in IV-VI and chalcogen (Se and Te) crystals was considered and it was suggested that "we might expect materials that exhibit resonance bonding in the crystalline phase to have different properties in the amorphous phase".

It was also stated that long-range order is crucial for resonance bonding to exist. If long-range order is lost, the system will be unable to achieve resonant bonding [204]. This approach has been subsequently elaborated in [188, 205, 206] to explain the unusually large property contrast in GST alloys.

There are two major differences between resonance bonding in molecules and phase-change alloys. While in the former, the bond lengths (and strengths) are identical, in the latter, there are shorter and longer bonds making resonance less likely. The second important difference is that in molecules resonance bonding exists in addition to the conventional covalent σ-bonds. As a result, the bond lengths get shorter, and stronger, then single covalent bonds. In this situation, even when the resonance interaction is broken, the structure remains stable because the primary covalent bonds persist. In phase-change materials, on the other hand, the longer bonds are formed at the expense of the shorter bond that are consequently longer than normal covalent bonds. In this case, when the resonance interaction is broken there will be no bonds between certain pairs of atoms making the structure locally unstable.
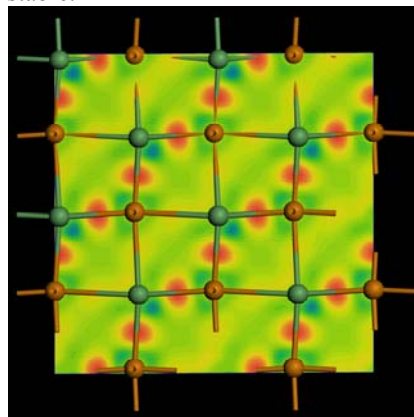

Fig. 15. Charge density difference map for binary GeTe. One can see that the charge pile-up indicative of covalent bonds only exists along the shorter Ge - Te bonds, after [207]

How does the bond length asymmetry effect the electron density distribution? The plot of the charge difference between the simulated relaxed GeTe model at 0K and isolated pseudo-atoms shown in Fig. 15 demonstrates that the electron density is only significant along the short bonds. In contrast, the electron density pile-up along the long bonds is significantly lower demonstrating that there is a pronounced bonding energy hierarchy between the short and long bonds [207]. The existing bonding energy hierarchy should manifest itself in the different response of the short and long bonds to thermal and/or electronic excitations. The fact that the long-range order is associated with the weak resonance bonding suggests that the crystalline phase is *intrinsically fragile*.

3.2.2. Amorphous phase

The amorphous phase of $Ge_2Sb_2Te_5$ has been studied by various groups [201, 202, 208, 209]. Using EXAFS (Fig. 16), it was found the Ge-Te bond to be 2.62 Å and the Sb-Te bond to be 2.84 Å (as compared to 2.83 Å and 2.94 Å, respectively, in the crystalline phase), i.e. the bonds are *shorter* in the amorphous phase. At the same time, the bond disorder was *smaller* in the amorphous phase. It is informative to note that the obtained Ge-Te and Sb-Te bond lengths are very close to the sum of the corresponding covalent radii for the elements (Ge = 1.22Å, Sb = 1.38 Å, Te= 1.35 Å). Shorter bonds in the as-deposited amorphous phase of $Ge_2Sb_2Te_5$ has also been observed by high-energy X-ray scattering experiments [210].
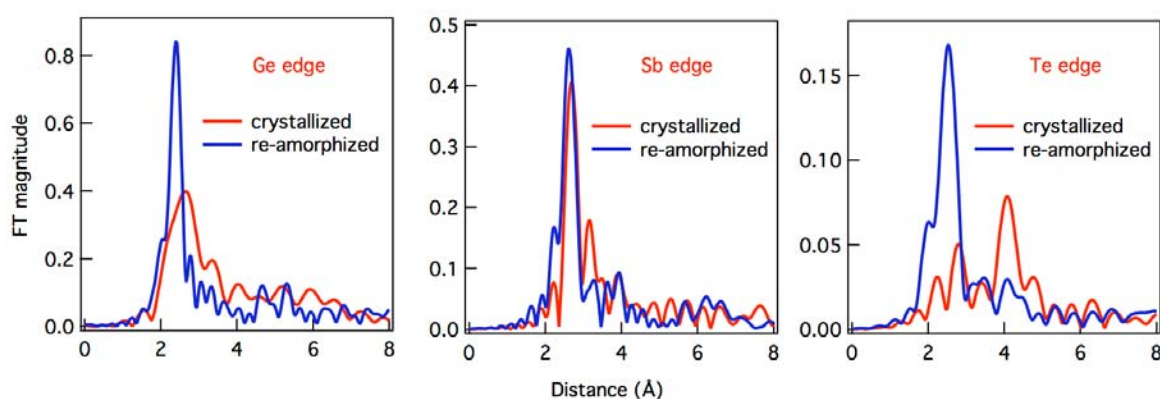

Fig. 16: Fourier-transformed K-edge EXAFS spectra for the crystallised and laser-amorphised $Ge_2Sb_2Te_5$ (after [202]).

The observed bond shortening and increased local order are highly unusual for covalent solids when, due to anharmonicity of the interatomic potential, disorder usually results in longer and weaker bonds and suggests that the local structures in the two cases are significantly different.

Use of X-ray absorption near-edge structure XANES, which is one of the very few methods sensitive to three-dimensional arrangement of atoms [202], confirmed the difference in the local structure (Fig. 17)
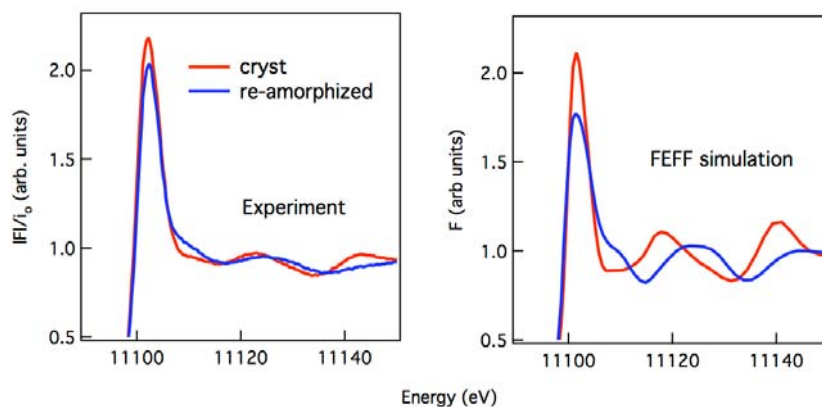

Fig. 17. Experimental (left) and simulated (right) Ge K-edge XANES spectra for the crystallised and laser-amorphised $Ge_2Sb_2Te_5$, after [202].

The overall observed changes in XANES upon the phase transition could be reproduced by FEFF simulations [211] when the Ge atoms were placed into tetrahedral symmetry sites [202] within the Te fcc lattice. Based on this finding the authors argued that the phase transition is triggered by an umbrella-flip of Ge atoms [202] between the octahedral and tetrahedral symmetry sites within the Te fcc lattice (Fig. 18). This provided the first atomistic explanation why the transition is so fast (a single atom switches) and why the medium is so stable (the Te sublattice is essentially preserved).
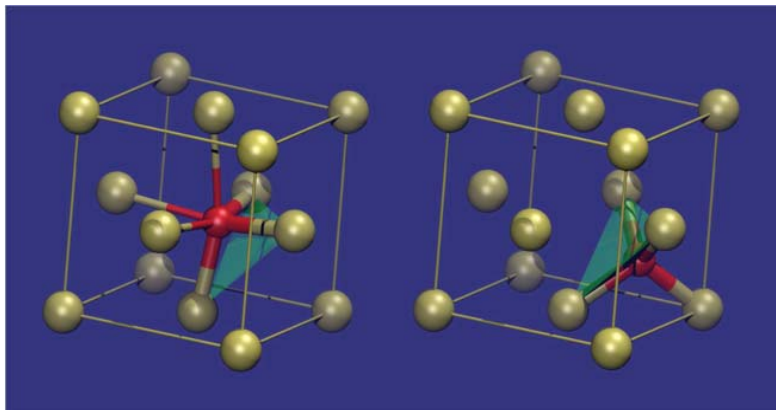

Fig. 18: Local structure around the central Ge atom for the crystalline (left) and amorphous (right) phases of Ge-Sb-Te, after [202].

A significant step forward was *in-silico* generation of a melt-quenched amorphous phase. The first simulation of the melt-quenched amorphous $Ge_2Sb_2Te_5$ was reported by Caravati et al. [212]. The liquid structure (270 atoms) generated at 2300 K was equilibrated for 6 ps and then quenched in 16 ps and further equilibrated for 18 ps at 990 K. In order to generate a model of a-$Ge_2Sb_2Te_5$, the liquid has been brought to 300 K in 18 ps. Subsequently these studies were extended [213].

The authors found Ge and Sb atoms were mostly four-fold coordinated and form bonds preferentially with Te atoms. A large fraction of Ge atoms were found on tetrahedral sites. Furthermore, the four-fold coordinated Ge distribution was found to be bimodal with peaks corresponding to defective octahedral and tetrahedral sites. For Te and Sb atoms no evidence of tetrahedral geometry was found. A similar result have been obtained using a much larger calculation cell [214]. The dominance of square fragments in the structure of the a-GST was subsequently observed from DFT simulations [214, 215]. Denoting Te atoms as ``A'' and Ge/Sb atoms as ``B'', the authors introduce ABAB squares as building blocks for the a-GST (Fig. 19)
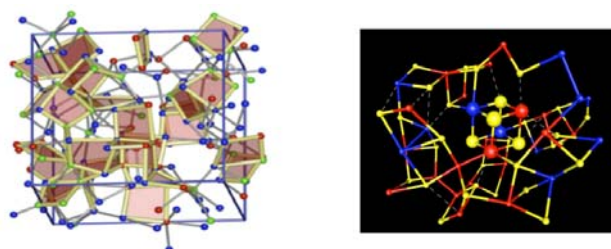

Fig. 19: Structure of melt-quenched amorphous phase of $Ge_2Sb_2Te_5$ obtained by ab-initio DFT simulations (left - after [215], right after [214]). Octahedrally coordinated Ge sites reminiscent of the crystalline phase are clearly visible.

It should be noted here that the coordination number used in most DFT studies assumed that there are covalent bonds between the central atom and its neighbors up to a specific cut-off distance}, usually around 3.2 Å. At the same time, the simple occurrence of a neighbor at a certain distance does not necessarily mean that there is a covalent bond between the atoms. Studies using isosurface plots of the charge difference between the simulated MQ amorphous model and isolated pseudo-atoms clearly demonstrate that the electron density that can be associated with a covalent bond is only significant between atoms whose distance is less than 3 Å [216] as shown in Fig. 20
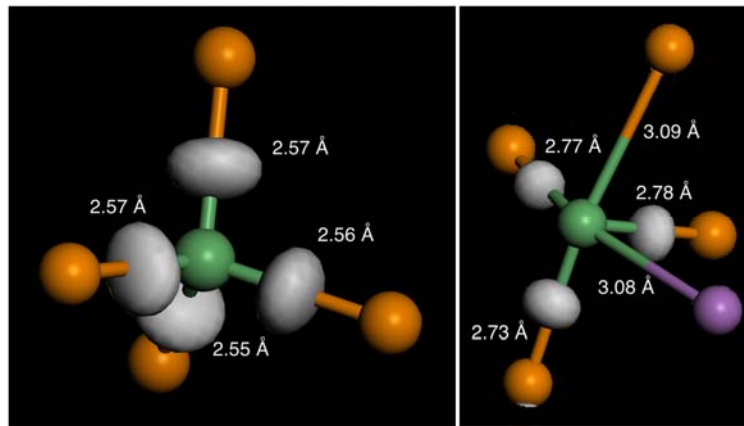
Fig. 20. Charge density difference (isosurfaces) for tetrahedrally (left) and octahedrally (right) coordinated Ge atoms in the amorphous phase of GST. One can see that an increase in electron density indicative of covalent bonds only exists for Ge-Te interatomic distances less than 3 Å [216].

3.3. Phase-change mechanism

3.3.1. Structural change between the two phases

The first model that attempted to provide an atomistic description of the phase-change process was the so-called umbrella-flip model [202], mentioned above. Within this model the crystal-to-amorphous transition consisted in a transformation of Ge local bonding geometry from (resonantly bonded) octahedral in the crystalline state to covalently bonded tetrahedral in the amorphous phase. It was suggested that this change in the bonding geometry was achieved through an umbrella flip of Ge atoms through a plane formed by Te atoms after the rupture of the longer Ge-Te bonds.

From the resonance bonding viewpoint, the structural change involved destruction of resonance resulting in a change of the bonding nature to pyramidally bonded covalent. The two models are similar in that both assume the rupture of the longer bonds as an initial stage of the process. The essential difference between the two is that in the latter case the formation of tetrahedral sites was deemed unnecessary: the process terminates after the resonance bonds are broken.
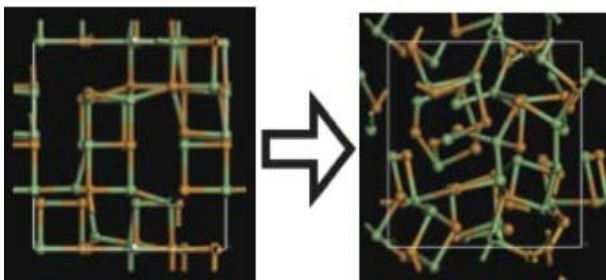

Fig. 21: The critically distorted crystalline GeTe phase (left) collapses and an amorphous phase is generated (right) (after [207]).

Since both experimental and simulational results found the existence of tetrahedral Ge sites, their presence is real but it should be noted that such sites are not necessarily obtained though the umbrella-flip but may also be formed when two Ge atoms located at apexes of adjacent pyramids come close to each other so that a Ge-Ge bond can be formed making Ge atoms tetrahedral. Not all pyramids acquire positions favourable for the formation of tetrahedral Ge sites limiting their fraction to about 30 %.

Loss of long-range order and and the formation of tetrahedral Ge sites though lattice relaxation has been demonstrated in [207] where it was shown that once the distortion exceeds a critical value, the structure spontaneously transforms into the amorphous phase (Fig. 21).

3.3.2. Role of electronic excitation

An important question arising is whether the above transformation result from purely thermal effects of a laser or current pulses or electronic excitation also plays a role? We would like to note that photo-induced loss of long-range order is not unusual. An $As_{50}Se_{50}$ film crystallised on a silica glass substrate becomes amorphous again if irradiated by continuous low-intensity light [217, 218]. This change is athermal because the light-induced heating is negligible.

It has also been found that selenium, in both amorphous and crystalline forms, can be melted by light at temperatures as low as 77 K [219]. Special care was taken to exclude the possibility that this effect is caused by heating due to light absorption. In particular, comparison of the Stokes and anti-Stokes peak intensities demonstrated that the temperature rise in this process did not exceed 10 degrees.

It was further found that the ``amorphous'' peak at 252 cm^{-1} was strongly polarised further underscoring the importance of electronic excitation. This result indicates that quasi-free chains produced as a result of photo

illumination are strongly oriented with respect to the polarisation of the excitation light. The authors concluded that photomelting of selenium is associated with breaking of interchain bonds between Se chains oriented parallel to the polarisation plane of the inducing light [219].

Athermal photomelting has also been studied by computer simulations and the obtained results suggested that ``the occupation of low-lying conduction states gives already weakly bonded atoms additional freedom to diffuse in the network and in extreme conditions to photomelting, while conventional thermal diffusion depends on the lattice dynamics of atoms'' [220].

While for the phase-change alloys the existing consensus is that light or current pulses serve uniquely to heat the materials, evidence of an importance of the electronic component is growing. Fig. 22 shows the time evolution of the white-line intensity of GST as a function of delay after the 500 ps excitation pulse [189]. One can clearly see from the figure that following exposure to the laser pulse the white-line intensity first monotonically decreases and reaches a minimum value in about 1 nanosecond. This fast initial decrease in white-line intensity is followed by its partial recovery and within ca. 2 ns a new saturation value is reached. This final value coincides with the value of the white-line intensity in the amorphous state.
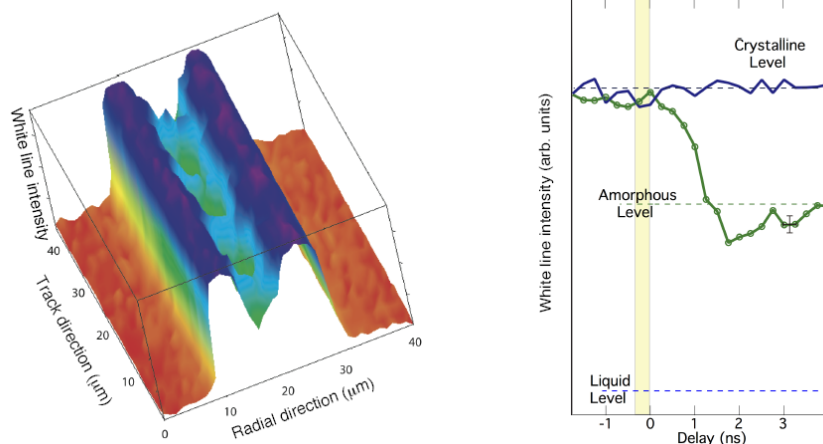

Fig. 22. Mapping of a crystallised track with amorphous bits using X-ray absorption (left) and evolution of the white-line intensity during the crystal-to-amorphous phase transition (right) demonstrating that the amorphisation does not involve conventional melting, after[189].

It is of particular interest that the minimum value of the white-line intensity during the amorphisation process is significantly higher than that corresponding to the static liquid state [221] clearly demonstrating that the material does not melt in a conventional sense upon its transformation from the crystalline to the amorphous phase and the amorphisation in the sub-nanosecond excitation regime may be a solid-solid process.

The role of electronic excitation in the phase-change process has also been investigated in [190] and it was concluded that electronic excitation considerably lowers the critical amorphisation temperature and reduces the atomic diffusion coefficient with respect to that of the corresponding liquid phase by at least one order of magnitude. Nonthermal amorphisation in GST induced by picosecond electric pulses has also been reported [191].

3.3.3. Origin of Optical Contrast

After the initial proposal of the umbrella-flip model that attributed the change in optical properties to a change in the local coordination of Ge atoms [201], Welnic et al. performed theoretical studies of the effect of the change in the Ge coordination number on the optical properties of phase change materials (both GeTe and GST124 were investigated). The amorphous state was modelled by putting all (or some of the) Ge atoms onto tetrahedral symmetry sites. For both materials, the experimentally observed changes in optical properties were qualitatively reproduced.

At the same time, the joint density of states alone in the two phases [220] could not explain the experimentally observed changes from which it was concluded that the optical contrast between the two phases can only be explained by significant changes in the transition matrix elements resulting from the changes in the number of bonds and in the local order upon the phase transition. A very similar conclusion was reached in [221].

Subsequent studies have demonstrated that optical contrast is primarily caused by misalignment of atoms that serves to break the resonance interaction [205]. Of interest is also an observation that the principal change in the optical properties takes place during the initial stage of the phase-change process when resonance bonding is ``turned off'' but the atomic structure still preserves the average long-range order of the crystalline phase. Subsequent

relaxation and loss of the long-range order results in a much smaller change in the optical properties [207]. In other words, the destruction of ``resonance'' bonding causes a major change in optical properties, while subsequent disordering of the structure that does not alter the covalent nature of bonding results in a minor change in optical properties. The above results show that optical properties are primarily determined by the nature of the bonding between the atoms, i.e. by the local rather than the average structure. In other words, the change in properties is caused by a change in the local bonding character rather than being due to the loss of long-range order.

3.4. Application: past, present, future

The R&D of phase-change optical storage has a long history starting with the discovery of the memory effect (a reversible change in resistivity) in some chalcogenide alloys by S.R. Ovshinsky [187]. In the late 1960s Hitachi began to study phase-change materials and in the early 1970s Matsushita Electric (Panasonic) initiated a similar research [224]. Matsushita Electric tested numerous compositions and eventually discovered in the late 1980s the promising Ge-Sb-Te alloys, and especially, the GST225 composition [225]. This work resulted in commercialisation of DVD-RAM by Hitachi and Matsushita Electric in 1998 [226, 227].

Fig. 23 shows the structure of a phase-change disc. All phase-change discs have the same structure: the bottom $ZnS-SiO_2$ layer used to control the maximum reflectivity level, a phase-change layer erasable recording, the top $ZnS-SiO_2$ film to enhance the optical contrast between the crystalline and amorphous states and an Al alloy layer to release heat accumulated in the phase-change film as quickly as possible.
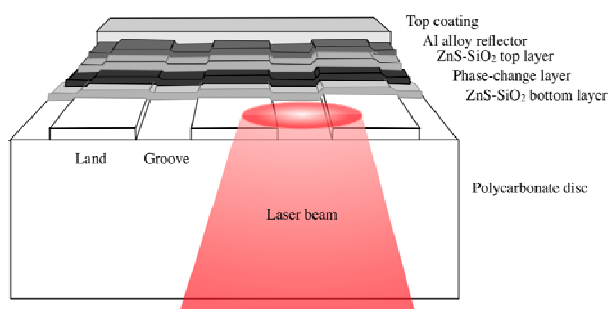

Fig. 23. Schematics of phase-change optical recording / readout.

Presently, the same phase-change alloys that are used in rewritable optical media are also the leading candidate for non-volatile phase-change random access memory (PCRAM). Samsung and Micron have started commercial production of such devices. Use of layered $GeTe-Sb_2Te_3$ structures where entropic losses during the phase change can be suppressed, allows to decrease energy consumption by over 90 % [228].

Finally it should be noted that GST, and layered $GeTe-Sb_2Te_3$ structures in particular, are topological

insulators (TI) [229, 230]. This is a new and very intensely investigated class of materials that are insulators in the bulk but due to a combination of strong spin-orbit coupling and time reversal symmetry possess topologically protected metallic surface states [231, 232]. This property opens a conceptually new possibilities of data storage by combining the ability of such materials to change phase and their TI properties in one of the phases, i.g. using external magnetic field or circularly polarised light. A discussion of TI properties of phase-change materials is beyond the scope of this work.

In this section, we have briefly discussed the current status of research on phase-change memory alloys. The interested readers can find more information in recent monographs [233, 234].

4. Conclusions

The mechanism of the observed transformations in glasses and glass-ceramics is believed to be associated with laser-induced melting and subsequent quenching of the material. In the case of phase-change alloys electronic excitation also plays a role, especially for untrashort laser pulses. Atomistic interpretations of the laser-induced amorphisation can be provided glasses in terms of amorphous materials being vacancy-mediated distortion of the crystalline structure.

Major advantages of laser-induced phase-structure modification is that that it is possible to remove a material without using ablation, and the possibility to change the material's locally by an appropriate processing conditions. Probably, this processing method will be of use in development of next-generation integrated devices. Research into photosensitive glasses as a special class of materials will promote discovery of other unique properties. In summary, coming nearer to knowledge of the fundamental mechanisms of laser processing could notably improve their accuracy and performance.

Development of a general-purpose element for photonics (similar to the invention of the semiconductor transistor in microelectronics), whose operation principle will be based on the phase transition from the amorphous to the crystalline state and back, is a great challenge and dramatic achievement of the future.

References

[1] A. V. Kolobov, Photo-induced metastabilty in amorphous semiconductors, Wiley-VCH, Weinheim (2003).
[2] K. Sugioka, Y. Cheng, K. Midorikawa, Appl. Phys. A. **81**, 1 (2005).
[3] T. Hongo, K. Sujioka, H. Niino, Y. Cheng, M. Masuda, I. Miyamoto, H. Takai, K. Midorikawa, J. Appl. Phys. **97**, 063517-1 (2005).
[4] M. Masuda, K. Sugioka, Y. Cheng, T. Hongo, K. Shihoyama, H. Takai, I. Miyamoto, K. Midorikawa, Appl. Phys A. **78**, 1029 (2004).

[5] Y. Hanada, K. Sugioka, H. Kawano, I.S. Ishikawa, A. Miyawaki, K. Midorikawa, Biomed. Microdevices. **10**, 403 (2008).

[6] Z. Wang, K. Sugioka, K. Midorikawa, Appl. Phys A. **89**, 951 (2007).

[7] M. Masuda, K. Sugioka, Y. Cheng, N. Aoki, M. Kawachi, K. Shihoyama, K. Toyoda, H. Helvajian, K. Midorikawa, Appl. Phys A. **78**, 857 (2003).

[8] F. E. Livingston, H. Helvajian, Photophysical processes that lead to ablation-free microfabrication in glass-ceramic materials in 3D laser microfabrication. Principles and Applications (Ed. by H. Misawa and S. Juodkazis), WILEY-VCH, Weinheim (2006).

[9] P. A. Skiba, V. P. Volkov, K. G. Predko, V. P. Veiko, Optical Engineering. **33**, 3572 (1994).

[10] V. P. Veiko, K. K. Kieu, Quantum Electronics. **37**, 92 (2007).

[11] V. P. Veiko, E. B. Yakovlev, E. A. Shakhno, Quantum Electronics. **39**, 185 (2009).

[12] T. Ohtsuka, M. Tsukamoto, Jap. J. Appl. Phys. **10**, 1045 (1971).

[13] A. Miniewic, J. Parka, S. Bartkiewic, A. Januszko, Pure and Appl. Opt. **7**, 179 (1998).

[14] L. Lucchetti, S. Di Bella, F. Simoni, Liquid Crystals. **29**, 515 (2002).

[15] N. V. Kamanina, M. M. Mikhailova, A. I. Denisyuk, I. Yu. Sapurina, Molecular Crystals and Liquid Crystals. **426**, 129 (2005).

[16] M. G. Tomilin, Proc. SPIE. **2051**, 286 (1993).

[17] D.-K. Yang, S.-T. Wu, Fundamentals of liquid crystal devices, John Wiley & Sons, Chichester (2006).

[18] J. R. Bradley, S. Kim, Metallurgical and Materials Transactions A. **19**, 2013 (1988).

[19] S. Metev, S. Savtchenko, K. Stamenov, V. Veiko, G. Kotov, G. Shandibina, IEEE J. Quantum Electron. **17**, 2004 (1981).

[20] V. P. Koronkevich, V. P. Kirianov, A. G. Poleshchuk, Proc. SPIE. **2363**, 290 (1995).

[21] V. P. Veiko, M. V. Yarchuk, A. I. Ivanov, J. Opt. Tech. **78**, 512 (2011).

[22] D. H. Auston, J. A. Golovchenko, P. R. Smith, C. M. Surko, T. N. C. Venkatesan, Appl. Phys. Lett. **33**, 1978 (1978).

[23] G. K. Celler, J. M. Poate, G. A. Rozgonyi, T. T. Sheng, J. Appl. Phys. **50**, 7264 (1979).

[24] J. Narayan, R. B. James, O. W. Holland, M. J. Aziz, J. Vac. Sci. Technol. A. **3**, 1836 (1985).

[25] W. Yang, P. G. Kazansky, Y. P. Svirko, Nature Photon. **2**, 99 (2008).

[26] R. R. Gattas, F. Mazur, Nature Photon. **2**, 219 (2008).

[27] Y. Cheng, K. Sugioka, K. Midorikawa, Appl. Surface Science. **248**, 172 (2005).

[28] Y. Cheng, K. Sugioka, K. Midorikawa, M. Masuda, K. Toyoda, M. Kawachi, K. Shihoyama, Optics Letters. **28**, 1144 (2003).

[29] D. Ashkenasi, H. Varel, A. Rosenfeld, S. Henz, J. Herrmann, E. E. B. Cambell, Appl. Phys. Lett. **72**, 1442 (1998).

[30] E. Ageev; K. Kieu; V. P. Veiko, Proc. SPIE. **7996**, 79960R (2010).

[31] S. K. Ahn, J. G. Kim, V. Perez-Mendez, S. Chang, K. H. Jackson, J. A. Kadyk, W. A. Wenzel, G. Cho, Nuclear Science. **49**, 870 (2002).

[32] T. R. Dietrich, M. Abraham, J. Diebel, M. Lacher, A. Ruf, J. Micromech. Microeng. **3**, 187 (1993).

[33] A. Ruf, J. Diebel, M. Abraham, T. R. Dietrich, M. Lacher, J. Micromech. Microeng. **6**, 254 (1996).

[34] J. Kim, Optics and Lasers in Engineering. **45**, 890 (2007).

[35] H. Becker, M. Arundell, A. Harnisch, D. Hulsenberg, Sens. Actuators j. B. **86**, 271 (2002).

[36] T. R. Dietrich, A. Freitag, R. Scholz, Chem. Eng. Technol. **28**, 1 (2005).

[37] K. Yunus, C. B. Marks, A. C. Fisher, D. W. E. Allsopp, T. J. Ryan, R. A. W. Dryfe, S. S. Hill, E. P. L. Roberts, C. M. Brennan, Electrochemistry Communications. **4**, 579 (2002).

[38] Knunyants I. L., Chemical encyclopedic dictionary, Soviet encyclopedia, Moscow (1983) [in Russian].

[39] N. Itoh and A.M. Stoneham, Materials Modification by Electronic Excitation, Cambridge University Press, 2001

[40] A. I. Berezhnoi, Glass Ceramics and Photo-Sitalls, Plenum Press, NY (1970).

[41] N. V. Nikonorov, E. I. Panysheva, I. V. Tunimanova, A. V. Chukharev, Glass Phys. and Chem. **27**, 241 (2001).

[42] S. D. Stookey, Ind. Eng. Chem. **41**, 856 (1949).

[43] K. Sugioka, Y. Cheng, K. Midorikawa, J. Phys.: Conf. Series. **59**, 533 (2007).

[44] C. G. K. Malek, Anal. Bioanal. Chem. **385**, 1362 (2006).

[45] H. Klank, J. P. Kutter, O. Geschke, Lab Chip. **2**, 242 (2002).

[46] Y. Cheng, Z. Xu, J. Xu, K. Sugioka, K. Midorikawa, The Review of Laser Engineering. **36**, 1206 (2008).

[47] T. R. Dietrich, W. Ehrfeld, M. Lacher, M. Kramer, B. Speit, Microelectron. Eng. **30**, 497 (1996).

[48] J. Brannon, J. Greer, H. Helvajian, Laser Processing for Microengineering Applications in Microengineering Aerospace Systems (Ed. by H. Helvajian), Aerospace Press, Reston (1999).

[49] A. J. Ikushima, T. Fujiwara, K. Saito, J. Appl. Phys. **88**, 373805-1 (2000).

[50] W. Holland, G. Beall, Glass-Ceramic Technology, Am. Ceram. Soc. Press, Westerville OH (2003).

[51] A. Marcinkevicius, S. Juodkazis, M. Watanabe, M. Miwa, S. Matsuo, H. Misawa, J. Nishii, Optics Letters. **26**, 277 (2001).

[52] K. M. Davis, K. Miura, K. Hirao, Optics Letters. **21**, 1729 (1996).

[53] Y. Bellouard, A. Said, M. Dugan, P. Bado, Opt. Express. **12**, 2120 (2004).

[54] C. Hnatovsky, R. S. Taylor, E. Simova, P. P. Rajeev, D. M. Rayner, V. R. Bhardwaj, P. B. Corkum, Appl. Phys. A. **84**, 47 (2006).

[55] B. Fisette, M. Meunier, J. of Laser Micro/Nanoengineering. **1**, 7 (2006).

[56] Z. Wang, K. Sugioka, K. Midorikawa, Appl. Phys. A. **93**, 225 (2008).

[57] Y. Cheng, K. Sugioka, K. Midorikawa, Proc. SPIE. **5662**, 209 (2004).

[58] DARPA/MTO/MEMS Digital Micro-Propulsion Project   http://design.caltech.edu/micropropulsion/foturan.html.

[59] M. Tashiro, N. Soga, S. Sakka, J. Ceram. Assoc. Japan. **87**, 169 (1960).

[60] Schott Corporation, Technical Glass Division, Yonkers, NY, Foturan product literature F10/1999.

[61] A. V. Kolobov, P. Fons, A. I. Frenkel, A. L. Ankudinov, J. Tominaga, T. Uruga, Nature Materials. **3**, 703 (2004).

[62] P. Fons, A. V. Kolobov, T. Fukaya, M. Suzuki, T. Uruga, N. Kawamura, M. Takagaki, H. Ohsawa, H. Tanida, J. Tominaga, Jap. J. Appl. Phys. **46**, 3711 (2007).

[63] J. Solis, C. N. Afonso, Appl. Phys. A. **76**, 331 (2003).

[64] S. M. Wiggins, J. Bonse, J. Solis, C. N. Afonso, K. Sokolowski-Tinten, V. V. Temnov, P. Zhou, D. von der Linde, J. Appl. Phys. **98**, 113518-1 (2005).

[65] J. Siegel, W. Gawelda, D. Puerto, C. Dorronsoro, J. Solis, C. N. Afonso, J. C. G. de Sande, R. Bez, A. Pirovano, C. Wiemer, J. Appl. Phys. **103**, 023516-1 (2008).

[66] W. Gawelda, J. Siegel, C. N. Afonso, V. Plausinaitiene, A. Abrutis, C. Wiemer, J. Appl. Phys. **109**, 123102-1 (2011).

[67] M. E. Fermann Ultrafast fiber oscillators in Ultrafast Lasers: Technology and Applications (Ed. by M. E. Fermann, A. Galvanauskas, G. Sucha), CRC Press, New York (2003).

[68] E. Gamaly, B. Luther-Davies, A. Rode, Laser–Matter Interaction Confined Inside the Bulk of a Transparent Solid in 3D laser microfabrication. Principles and Applications (Ed. by H. Misawa and S. Juodkazis), WILEY-VCH, Weinheim (2006).

[69] Y. Shimotsuma, M. Sakakura, M. Shimizu, K. Miura, P. G. Kazansky, K. Hirao, Proc. SPIE. **6985**, 698503-1 (2008).

[70] C. B. Schaffer, A. Brodeur, J.F. García, E. Mazur, Optics Letters. **26**, 93 (2001).

[71] M. Bellec, A. Royon, B. Bousquet, K. Bourhis, M. Treguer, T. Cardinal, M. Richardson, L. Canioni, Opt. Express. **17**, 10304 (2009).

[72] S. H. Cho, H. Kumagai, K. Midorikawa, Nucl. Instrum. Methods Phys. Res. B. **197**, 73 (2002).

[73] K. Minoshima, A. M. Kowalevicz, I. Hartl, E.P. Ippen, J. G. Fujimoto, Optics Letters. **26**, 1516 (2001).

[74] M. Talkenberg, E. W. Kreutz, A. Horn, M. Jacquorie, R. Poprawe, Proc. SPIE. **4637**, 258 (2002).

[75] W. W Hansen, S.W. Janson, H. Helvajian, Proc. SPIE. **2991**, 104 (1997).

[76] J. M. Fernandez-Pradas, D. Serrano, P. Serra, J.L. Morenza, Appl. Surface Science. **255**, 5499 (2009).

[77] J. Kim, H. Berberoglu, X. Xu, J. of Microlithography Microfabrication and Microsystems. **3**, 478 (2004).

[78] J. M. Fernández-Pradas, D. Serrano, S. Bosch, J. L. Morenza, P. Serra, Appl. Surface Science. **257**, 5219 (2011).

[79] F. E. Livingston, H. Helvajian, Proc. SPIE. **4830**, 189 (2003).

[80] P. D. Fuqua, D. P. Taylor, H. Helvajian, W. W. Hansen, M. H. Abraham, Mater. Res. Soc. Proc. **624**, 79 (2000).

[81] F. E. Livingston, P. M. Adams, H. Helvajian, Proc. SPIE. **5662**, 44 (2004).

[82] P. M. Adams, H. Helvajian, Appl. Surface Science. **247**, 526 (2005).

[83] B. Fisette, F. Busque, J-Y. Degorce, M. Meunier, Appl. Phys Lett. **88**, 091104-1 (2006).

[84] F. E. Livingston, H. Helvajian Photophysical processes that activate selective changes in photostructurable glass ceramic material properties in Photon-based nanoscience and nanobiotechnology (Ed. by J. J. Dubowski and S. Tanev), Springer, Berlin (2007).

[85] S. D. Stookey, Ind. Eng. Chem. **45**, 115 (1953).

[86] J. Qiu, M. Shirai, T. Nakaya, J. Si, X. Jiang, C. Zhu, K. Hirao, Appl. Phys. Lett. **81**, 3040 (2002).

[87] V. P. Veiko, G. K. Kostyuk, N. V. Nikonorov, A. N. Rachinskaya, E. B. Yakovlev, D. V. Orlov, Proc. SPIE. **6606**, 66060Q-1 (2007).

[88] V. P. Veiko, A. I. Ignatyev, N. V. Nikonorov, E. B. Yakovlev, D. V. Orlov, Proc. SPIE. **6985**, 69850E-1 (2008).

[89] V. P. Volkov, P. A. Skiba, A. G. Sechko, A. G. Nepokoychitsky, Glass Phys. and Chem. **17**, 242 (1991) [in Russian].

[90] V. P. Veiko, N. V. Nikonorov, P. A. Skiba, J. Opt. Tech. **73**, 419 (2006).

[91] V. Veiko, E. Shakhno, E. Yakovlev, B. Novikov, Proc. of SPIE. **6985**, 69850C-1 (2008).

[92] V. Veiko, E. Shakhno, E. Yakovlev, B. Novikov, Laser Physics. **18**, 363 (2008).

[93] C. J. Anthony, P. T. Docker, P. D. Prewett, K. Jiang, J. Micromech. Microeng. **17**, 115 (2007).

[94] I. Gomez-Morilla, M. H. Abraham, D. G. de Kerckhove, G. W. Grime, J. Micromech. Microeng. **15**, 706 (2005).

[95] A. A. Bettiola, S. Venugopal Rao, T. C. Suma, J. A. van Kana, F. Watta, J. of Crystal Growth. **288**, 209 (2006).

[96] K. Miura, J. Qiu, H. Inouye, T. Mitsuyu, K. Hirao, Appl. Phys. Lett. **71**, 3329 (1997).

[97] Y. Kondo, T. Suzuki, H. Inouye, K. Miura, T. Mitsuyu, K. Hirao, Jap. J. Appl. Phys. **37**, L94 (1998).

[98] M. Will, S. Nolte, B. N. Chichkov, A. Tunnermann, Appl. Opt. **41**, 4360 (2002).

[99] A. Zoubir, M. Richardson, L. Canioni, A. Brocas, L. Sarger, J. Opt. Soc. Am. B. **22**, 2138 (2005).

[100] D. Homoelle, S. Wielandy, A. L. Gaeta, N. F. Borrelli, C. Smith, Optics Letters. **24**, 1311 (1999).

[101] O. M. Efimov, L. B. Glebov, K. A. Richardson, E. van Stryland, T. Cardinal, S. H. Park, M. Couzi, J. L. Bruneel, Opt. Mater. **17**, 379 (2001).

[102] E. N. Glezer, M. Milosavljevic, L. Huang, R. J. Finlay, T.-H. Her, J. P. Callan, E. Mazur, Optics Letters. **21**, 2023 (1996).

[103] L. Canioni, M. Bellec, A. Royon, B. Bousquet, T. Cardinal, Optics Letters. **33**, 360 (2008).

[104] J. Qiu, K. Miura, K. Hirao, Jap. J. Appl. Phys. **37**, 2263 (1998).

[105] S. Kawata, H.B. Sun, T. Tanaka, K. Takada, Nature. **412**, 697 (2001).

[106] S. Nolte, M. Will, J. Burghoff, A. Tuennermann, Appl. Phys. A. **77**, 109 (2003).

[107] D. N. Fittinghoff, C. B. Schaffer, E. Mazur, J. A. Squier, IEEE J. Sel. Top. Quantum Electron. **7**, 559 (2001).

[108] J. R. Liu, Z. Y. Zhang, S. D. Chang, C. Flueraru, C. P. Grover, Opt. Commun. **253**, 315 (2005).

[109] D. K. Y. Low, H. Xie, Z. Xiong, G. C. Lim, Appl. Phys. A. **81**, 1633 (2005).

[110] A. M. Streltsov, N. F. Borrelli, Optics Letters. **26**, 42 (2001).

[111] K. Minoshima, A. M. Kowalevicz, E. P. Ippen, J. G. Fujimoto, Opt. Express. **10**, 645 (2002).

[112] W. Watanabe, T. Asano, K. Yamada, K. Itoh, J. Nishii, Optics Letters. **28**, 2491 (2003).

[113] T. Pertsch, U. Peschel, F. Lederer, J. Burghoff, M. Will, S. Nolte, A. Tunnermann, Optics Letters. **29**, 468 (2004).

[114] A. M. Kowalevicz, V. Sharma, E. P. Ippen, J. G. Fujimoto, K. Minoshima, Optics Letters. **30**, 1060 (2005).

[115] A. Martinez, M. Dubov, I. Khrushchev, I. Bennion, Electron. Lett. **40**, 1170 (2004).

[116] Y. Kondo, K. Nouchi, T. Mitsuyu, M. Watanabe, P. G. Kazansky, K. Hirao, Optics Letters. **24**, 646 (1999).

[117] Y. Li, W. Watanabe, K. Yamada, T. Shinagawa, K. Itoh, J. Nishii, Y. Jiang, Appl. Phys. Lett. **80**, 1508 (2002).

[118] N. Takeshima, Y. Narita, S. Tanaka, Y. Kuroiwa, K. Hirao, Optics Letters. **30**, 352 (2005).

[119] K. C. Vishnubhatla, S. Venugopal Rao, R. Sai Santosh Kumar, K. Shiva Prasad, P. S. R. Prasad, D. Narayana Rao, Proc. SPIE. **6881**, 688113-1 (2008).

[120] J. Liu, Z. Zhang, Z. Lu, G. Xiao, F. Sun, S. Chang, C. Flueraru, Appl. Phys. B. **86**, 151 (2007).

[121] R. Osellame, S. Taccheo, M. Marangoni, R. Ramponi, P. Laporta, D. Polli, S. De Silvestri, G. Cerullo, J. Opt. Soc. Am. B. **20**, 1559 (2003).

[122] Y. Sikorski, A. A. Said, P. Bado, R. Maynard, C. Florea, K. A. Winick, Electron. Lett. **36**, 226 (2000).

[123] N. D. Psaila, R. R. Thomson, H. T. Bookey, A. K. Kar, N. Chiodo, R. Osellame, G. Cerullo, A. Jha, S. Shen, Appl. Phys. Lett. **90**, 131102-1 (2007).

[124] E. Bricchi, J. D. Mills, P. G. Kazansky, B. G. Klappauf, J. J. Baumberg, Optics Letters. **27**, 2200 (2002).

[125] J. Qiu, K. Miura, H. Inouye, Y. Kondo, T. Mutsuyu, K. Hirao, Appl. Phys. Lett. **73**, 1763 (1998).

[126] M. Ams, G.D. Marshall, P. Dekker, M. Dubov, V. K. Mezentsev, I. Bennion, M. J. Withford, IEEE J. Sel. Top. Quantum Electron. **14**, 1370 (2008).

[127] W. W. Hansen, S. W. Janson, H. Helvajian, Proc. SPIE. **2991**, 104 (1997).

[128] F. E. Livingston, H. Helvajian, Appl. Phys. A. **81**, 1569 (2005).

[129] F. E. Livingston, H. Helvajian, J. of Photochemistry and Photobiology A: Chemistry. **182**, 310 (2006).

[130] Y. Cheng, K. Sugioka, K. Midorakawa, M. Masuda, K. Toyoda, M. Kawachi, K. Shihoyama, Optics Letters. **28**, 1144 (2003).

[131] K. H. M. Tantawi, J. Oates, R. Kamali-Sarvestani, N. Bergquist, J. D. Williams, J. Micromech. Microeng. **21**, 017001-1 (2011).

[132] T. R. Dietrich, W. Ehrfeld, M. Lacher, M. Krämer, B. Speit, Microelectron. Eng. **30**, 497 (1996).

[133] P. Fuqua, S. W. Janson, W. W. Hansen, H. Helvajian, Proc. SPIE. **3618**, 213 (1999).

[134] W. W. Hansen, S. W. Janson, H. Helvajian, Proc. SPIE. **2991**, 104 (1997).

[135] F. E. Livingston, W. W. Hansen, A. Huang, H. Helvajian, Proc. SPIE. **4637**, 404 (2002).

[136] R. M. Karam, R.J. Casler, http://www.invenios.com/resources.html

[137] P. S. Dittrich, K. Tachikawa, A. Manz, Anal. Chem. **78**, 3887 (2006).

[138] Y. J. Bellouard, A. Said, P. Bado, Opt. Express. **13**, 6635 (2005).

[139] V. Lien, K. Zhao, Y.H. Lo, Appl. Phys Lett. **87**, 194106-1 (2005).

[140] V. R. Bhardwaj, E. Simova, P. B. Corkum, D. M. Rayner, C. Hnatovsky, R. S. Taylor, B. Schreder, M. Kluge, J. Zimmer, J. Appl. Phys. **97**, 083102-1 (2005).

[141] J. W. Chan, T .R. Huser, S. H. Risbud, J. S. Hayden, D. M. Krol, Appl. Phys. Lett. **82**, 2371 (2003).

[142] S. Balslev, A. Kristensen, Opt. Express. **13**, 344 (2005).

[143] U. Cheng, K. Sugoka, M. Masusa, K. Shihoyama, K. Toyoda, K. Midorikawa, Opt. Express. **11**, 1809 (2003).

[144] L. Yan, W. Wataru, Y. Kazuhiro, S. Taishi, I. Kazuyoshi, N. Junji, J. Yongyuan, Appl. Phys. Lett. **80**, 1508 (2002).

[145] Y. Cheng, K. Sugioka, K. Midorikawa, Opt. Express. **13**, 7225 (2005).

[146] Y. Cheng, K. Sugioka, K. Midorikawa, Optics Letters. **29,** 2007 (2004).

[147] Y. Cheng, H .L. Tsai, K. Sugioka, K. Midorikawa, Appl. Phys. A. **85**, 11 (2006).

[148] D. J. Hwang, M. Kim, K. Hiromatsu, H. Jeon, C. P. Grigoropoulos, Appl. Phys. A. **96**, 385 (2009).

[149] J. Pihl, J. Sinclair, M. Karlsson, O. Orwar, Materials Today. **8**, 46 (2005).

[150] H. Becker, C. Gartner, Anal. Bioanal. Chem. **390**, 89 (2008).

[151] D. Mijatovic, J. C. T. Eijkel, A. van den Berg, Lab Chip. **5**, 492 (2005).

[152] P. Gould, Materials today. **7**, 48 (2004).

[153] D. S. Shin, J. H. Lee, J. Suh, T. H. Kim, Opt. Laser Eng. **44**, 615 (2006).

[154] W. Pfleging, T. Hanemann, W. Bernauer, M. Torge, Proc. SPIE. **4637**, 318 (2002).

[155] L. J. Heydermann, H. Schift, C. David, B. Ketterer, M. Auf der Maur, J. Gobrecht, Microelectron Eng. **5758**, 375 (2001).

[156] X. D. Huang, L. R. Bao, X. Cheng, L.J. Guo, S. W. Pang, A. F. Yee, J. Vac. Sci. Technol. B. **20**, 2872 (2002).

[157] M. T. Gale, C. Gimkiewicz, S. Obi, M. Schnieper, J. Sochtig, H. Thiele, S. Westenhöfer, Opt. Laser Eng. **43**, 373 (2005).

[158] S. Y. Chou, P. R. Krauss, Microelectron. Eng. **35**, 237 (1997).

[159] Y. Kikutani, T. Horiuchi, K. Uchiyama, H. Hisamoto, M. Tokeshi, T. Kitamori, Lab Chip. **2**, 188 (2002).

[160] C. W. Cheng, J. S. Chen, P. X. Lee, C. W. Chien, Optics and Lasers in Engineering. **48**, 811 (2010).

[161] D. J. Hwang, M.·Kim, K. Hiromatsu, H. Jeon, C.P. Grigoropoulos, Appl. Phys. A. **96**, 385 (2009).

[162] V. Maselli, R. Osellame, G. Cerullo, R. Ramponi, P. Laporta, L. Magagnin, P.L. Cavallotti, Appl. Phys. Let. **88**, 191107-1 (2006).

[163] J.-Y. Cheng, M.-H. Yen, C.-W. Wei, Y.-C. Chuang, T.-H. Young, J. Micromech. Microeng. **15**, 1147 (2005).

[164] Y. Wu, W. Jia, C. Wang, M.·Hu, X.·Ni, L. Chai, Opt. Quant. Electron. **39**, 1223 (2007).

[165] Y. Kondo, J. Qiu, T. Mitsuyu, K. Hirao, T. Yoko, Jap. J. Appl. Phys. **38**, L1146 (1999).

[166] A. Crespi, Y. Gu, B. Ngamsom, H. J. W. M. Hoekstra, C. Dongre, M. Pollnau, R. Ramponi, H. H. van den Vlekkert, P. Watts, G. Cerulloa, R. Osellame, Lab Chip. **10**, 1167 (2010).

[167] M. Sakakura, M. Terazima, K. Miura, Y. Shimotsuma, K. Hirao, Proc. SPIE. **6985**, 698509-1 (2007).

[168] H. B. Sun, Y. Xu, S. Juodkazis, K. Sun, M. Watanabe, S. Matsuo, H. Misawa, J. Nishii, Optics Letters. **26**, 325 (2001).

[169] F. He, H. Sun, M. Huang, J. Xu, Y. Liao, Z. Zhou, Y. Cheng, Z. Xu, K. Sugioka, K. Midorikawa, Appl. Phys. A. **97**, 853 (2009).

[170] E. Toratani, M. Kamata, M. Obara, Appl. Phys. Lett. **87**, 171103-1 (2005).

[171] H. Sun, J. Song, C. Li, J. Xu, X. Wang, Y. Cheng, Z. Xu, J. Qiu, T. Jia, Appl. Phys. A. **88**, 285 (2007).

[172] V. R. Bhardwaj, E. Simova, P. B. Corkum, D. M. Rayner, C. Hnatovsky, R. S. Taylor, B. Schreder, M. Kluge, J. Zimmer, J. Appl. Phys. **97**, 083102 (2005).

[173] M. Masuda, K. Sugioka, Y. Cheng, N. Aoki, M. Kawachi, K. Shihoyama, K. Toyoda, K. Midorikawa, Proc. SPIE. **4830**, 576 (2002).

[174] S. Ho, P. R. Herman, Y. Cheng, K. Sujioka, K. Midorikawa, Proc. Conf. on Lasers and Electro-Optics, San Francisco, CA, USA, 2004, p. CThD6.

[175] V. P. Veiko, Q. K. Kieu, Proc. of SPIE. **5399**, 11 (2004).

[176] P. Volkov, A. I. Nepokoychitsky, A. G. Sechko, P. A. Skiba, Local modification of sitals and Ti–glasses under laser action, Belarus. Ac. of Sci., Minsk (1996) [in Russian].

[177] V. P. Veiko, K. A. Predko, V. P. Volkov, P. A. Skiba, Proc. SPIE. **1751**, 361 (1992).

[178] V. P. Veiko, Q. K. Kieu, N. V. Nikonorov, Proc. SPIE. **5662**, 119 (2004).

[179] H. Murotani, M. Wakaki, S. Kawabata, K. Nakamoto, Proc. SPIE. **5525**, 226 (2004).

[180] S. Calixto, M. Rosete-Aguilar, F. J. Sanchez-Marin, L. Castañeda-Escobar, Appl. Opt. **44**, 4547 (2005).

[181] M. Ornelas-Rodriguez, S. Calixto, Optical Engineering. **40**, 921 (2001).

[182] K. Kawamura, M. Hirano, T. Kamiya, H. Hosono, Appl. Phys. Let. **81**, 1137 (2002).

[183] S.-H. Cho, H. Kumagai, K. Midorikawa, Nucl. Instrum. Methods Phys. Res. B. **197**, 73 (2002).

[184] M. Kosters, H-T. Hsieh, D. Psaltis, K. Buse, Appl. Opt. **44**, 3399 (2005).

[185] O. M. Efimov, L. B. Glebov, V .I. Smirnov, Proc. SPIE. **4452**, 39 (2001).

[186] L. B. Glebov, Glass Science and Technology. **75**, 73 (2002).

[187] S. R. Ovshinsky, Phys. Rev. Lett. 21, 1450 (1968).

[188] K. Shportko, S. Kremers, M. Woda, D. Lencer, J. Robertson, and M. Wuttig, Nature Mater. **7**, 653 (2008).

[189] P. Fons, H. Osawa, A. V. Kolobov, T. Fukaya, M. Suzuki, T. Uruga, N. Kawamura, H. Tanida, J. Tominaga, Phys. Rev. B **82**, 041203 (2010).

[190] X.-B. Li, X. Q. Liu, X. Liu, D. Han, Z. Zhang, X. D. Han, H.-B. Sun, S. B. Zhang, Phys. Rev. Lett. **107**, 015501 (2011).

[191] D. Q. Huang, X. S. Miao, Z. Li, J. J. Sheng, J. J. Sun, J. H. Peng, J. H. Wang, Y. Chen, X. M. Long, Appl. Phys. Lett. **98**, 242106 (2011).

[192] P. Littlewood, J. Phys. C. **13**, 4855 (1980).

[193] J.-P. Gaspard, A. Pellegatti, F. Marinelli, C. Bichara, Philos. Mag. B **77**, 727 (1998).

[194] T. Chattopadhyay, J. Boucherle, H. Von Schnering,
      J. Phys. C **20**, 1431 (1987).

[195] P. Fons, A. V. Kolobov, M. Krbal, J. Tominaga,
      K. S. Andrikopoulos, S. N. Yannopoulos,
      G. A. Voyiatzis, and T. Uruga, Phys. Rev.
      B **82**, 155209 (2010).

[196] T. Matsunaga, P. Fons, A. V. Kolobov, J. Tominaga,
      N. Yamada, App. Phys. Lett. **99**, 231907 (2011).

[197] N. Yamada, MRS Bull. **21**, 48 (1996).

[198] N. Yamada, T. Matsunaga, J. Appl. Phys.
      88, 7020 (2000).

[199] T. Nonaka, G. Ohbayashi, Y. Toriumi, Y. Mori,
      H. Hashimoto, Thin Solid Films **370**, 258 (2000).

[200] T. Matsunaga, R. Kojima, N. Yamada, K. Kifune,
      Y. Kubota, Y. Tabata, M. Takata, Inorg. Chem.
      45, 2235 (2006).

[201] B. Hyot, X. Biquard, and L. Poupinet,
      in Proceedings of the European Phase Change
      Symposium (2001).

[202] A. V. Kolobov, P. Fons, A. I. Frenkel,
      A. L. Ankudinov, J. Tominaga, T. Uruga, Nature
      Mater. **3**, 703 (2004).

[204] S. Shamoto, N. Yamada, T. Matsunaga, T. Proffen,
      J. W. Richardson, J.-H. Chung, T. Egami, Appl.
      Phys. Lett. **86**, 081904 (2005).

[205] G. Lucovsky and R. White, Phys. Rev.
      B **8**, 660 (1973).

[206] J. Robertson, K. Xiong, and P. W. Peacock, Thin
      Solid Films **515**, 7538 (2007).

[207] B. Huang and J. Robertson, Phys. Rev.
      B **81**, 081204R (2010).

[208] A. V. Kolobov, M. Krbal, P. Fons, J. Tominaga,
      T. Uruga, Nature Chem. **3**, 311 (2011).

[209] D. A. Baker, M. A. Paesler, G. Lucovsky,
      P. C. Taylor, J. Non-Cryst. Solids **352**, 1621 (2006).

[210] P. Jovari, I. Kaban, J. Steiner, B. Beuneu,
      A. Schops, M. A. Webb, Phys. Rev.
      B **77**, 035202 (2008).

[211] S. Kohara, K. Kato, S. Kimura, H. Tanaka, T. Usuki,
      K. Suzuya, H. Tanaka, Y. Moritomo, T. Matsunaga,
      N. Yamada, et al., Appl. Phys. Lett.
      89, 201910 (2006).

[212] A. L. Ankudinov, B. Ravel, J. J. Rehr,
      S. D. Conradson, Phys. Rev. B **58**, 7565 (1998).

[213] S. Caravati, M. Bernasconi, T. Ku'hne, M. Krack,
      M. Parrinello, Appl. Phys. Lett. **91**, 171906 (2007).

[214] S. Caravati, M. Bernasconi, T. Ku 'hne, M. Krack,
      M. Parrinello, J. Phys: Cond. Matter
      21, 255501 (2009).

[215] J. Akola, R. O. Jones, Phys. Rev.
      B **76**, 235201 (2007).

[216] J. Hegedus S. R. Elliott, Nature Mater.
      7, 399 (2008).

[217] M. Krbal, A. V. Kolobov, P. Fons, J. Tominaga,
      S. R. Elliott, J. Hegedus, T. Uruga, Phys. Rev.
      B **83**, 054203 (2011).

[218] S. R. Elliott, A. V. Kolobov, J. Non-Cryst. Solids
      128, 216 (1991).

[219] A. V. Kolobov, S. R. Elliott, J. Non-Cryst. Solids
      189, 297 (1995).

[220] V. V. Poborchii, A. V. Kolobov, K. Tanaka, Appl.
      Phys. Lett. **74**, 215 (1999).

[221] J. Li, D. A. Drabold, Phys. Rev. Lett.
      85, 2785 (2000).

[222] A. V. Kolobov, P. Fons, M. Krbal, R. E. Simpson,
      S. Hosokawa, T. Uruga, H. Tanida,
      J. Tominaga, Appl. Phys. Lett. **95**, 241902 (2009).

[223] W. Welnic, S. Botti, L. Reining, M. Wuttig, Phys.
      Rev. Lett. **98**, 236403 (2007).

[224] S. Caravati, M. Bernasconi, M. Parrinello, J. Phys:
      Cond. Matter **22**, 315801 (2010).

[225] M. Terao, T. Morikawa, T. Ohta, Jpn. J. App. Phys.
      48, 080001 (2009).

[226] N. Yamada, E. Ohno, N. Akahira, K. Nishiuchi,
      K. Nagata, M. Takao, Jpn. J. Appl. Phys
      26S4, 61 (1987).

[227] H. Kitaura, E. Ohno, K. Nishiuchi, N. Ya- mada,
      in Proc. of the 11th Symp. Phase change Optical
      Information Storage (PCOS'99) (Mishima, Japan,
      1999), p. 89.

[228] T. Ohta, J. Optoelectron. Adv. Mater. **3**, 609 (2001).

[229] R. E. Simpson, P. Fons, A. V. Kolobov, T. Fukaya,
      M. Krbal, T. Yagi, J. Tominaga, Nature Nanotech.
      6, 501 (2011).

[230] J. Kim, J. Kim, and S.-H. Jhi, Phys. Rev.
      B **82**, 201312 (2010).

[231] J. Tominaga, R. E. Simpson, P. Fons,
      A. V. Kolobov, Appl. Phys. Lett.
      99, 152105 (2011).

[233] M. Z. Hasan, C. L. Kane, Rev. Mod. Phys.
      82, 3045 (2010).

[234] J. E.Moore, Nature **464**, 194 (2010).

[235] S. Raoux, M. Wuttig, eds., Phase Change
      Materials: Science and Applications (Springer
      Verlag, 2008).

[236] A. V. Kolobov, J. Tominaga, Chalcogenides:
      metastability and phase-change phenomena,
      Springer Verlag, 2012.

*Corresponding author: a.kolobov@aist.go.jp